CEBAF-PR-93-035
October 21, 1993

LEPTONIC PRODUCTION OF BARYON RESONANCES*

Volker D. Burkert
CEBAF
12000 Jefferson Avenue, Newport News,
Virginia 23606, USA

*Lectures presented at the Advanced Summer Study, Dronten,
The Netherlands, August 1-14, 1993

CONTINUOUS ELECTRON BEAM ACCELERATOR FACILITY

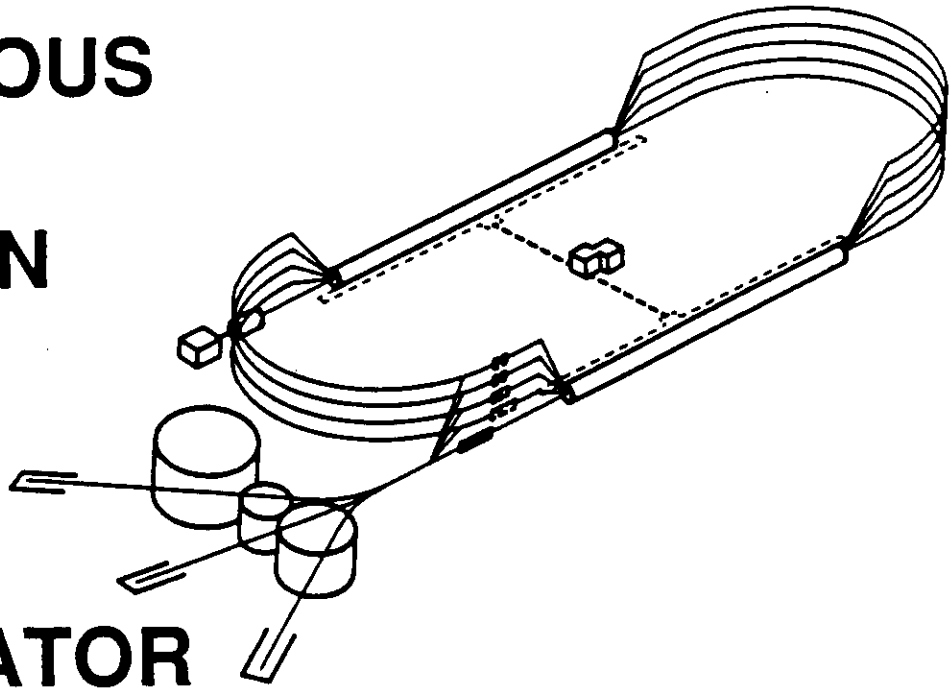

SURA ***Southeastern Universities Research Association***

CEBAF
The Continuous Electron Beam Accelerator Facility
Newport News, Virginia

Copies available from:

Library
CEBAF
12000 Jefferson Avenue
Newport News
Virginia 23606

The Southeastern Universities Research Association (SURA) operates the Continuous Electron Beam Accelerator Facility for the United States Department of Energy under contract DE-AC05-84ER40150.

LEPTONIC PRODUCTION OF BARYON RESONANCES

Volker D. Burkert

Continuous Electron Beam Accelerator Facility
12000 Jefferson Avenue, Newport News,
Virginia 23606, USA

INTRODUCTION

The quest for understanding the structure and interaction of hadrons has been the main motivation of strong interaction physics for decades. The advent of Quantum Chromodynamics (QCD) has led to a theoretical description of the strong interaction in terms of the fundamental constituents, quarks and gluons. However, we are still a long way from having the general theoretical framework in place to understand the strong force as it is manifest in the structure of complex hadronic systems such as baryons. At very high energies, perturbative methods have proven very effective. At low energies, simulations on the QCD lattice have generated remarkable results about the static properties of hadrons. Even calculations of electromagnetic form-factors have been possible at low momentum transfers. However, for light quark baryons such as nucleons, the small quark masses are difficult to implement, and crude approximations have been necessary.

Chiral perturbation theory is an attempt to apply QCD at low energies. In a well defined kinematical regime, for example close to the pion production threshold, it is possible to perform model independent calculations. However, even there resonance contributions give sizeable corrections, which at the present time cannot be calculated reliably.

In the forseeable future, models of the hadron structure will likely continue to play an important role and provide theoretical guidance to experimenters. The QCD inspired non-relativistic quark model[1] has been extended to include relativistic corrections in a consistent way[2] and applied successfully to the calculation of photoproduction amplitudes[3]. Other, conceptually completely different approaches are being pursued such as algebraic models[4]. The Skyrme model applied to photoproduction[5] can be used to calculate the complete partial wave amplitudes of the process $\gamma N \rightarrow \pi N$. However, in this description the electromagnetic vertex cannot be isolated from the hadronic vertex and the power of the electromagnetic interaction as a probe of the

hadronic structure is lost, at least to some degree.

Today's challenge in strong interaction physics at intermediate energies is to obtain a *detailed* understanding of the hadronic structure of matter. In other words, given QCD, how are hadrons made up of fundamental constituents, quarks and gluons?

Nucleons are probably the most common form of hadronic matter in the universe. Understanding their internal structure will give us insight into how the real world works. Nucleons can be probed in a number of ways which are sensitive to different aspects of the nucleon substructure:

- electromagnetic and weak elastic formfactors describe the electromagnetic and weak charge and current distributions of the ground state proton and neutron, providing information about the ground state wavefunction.

- the nucleon excitation spectrum is another important source of information about its internal structure. Existence or non-existence of certain states gives information about the underlying symmetry properties of the nucleon. The excitation spectrum may be probed with pion beams for those states that have an appreciable coupling to the πN channel. Electromagnetic excitation of resonances yields both overlapping and complementary information to pion scattering as some states may couple only weakly to pions or to photons.

- electroproduction of resonances is a unique means of probing the quark wavefunction of the excited states, provided the wavefunction of the ground state is known. In addition, photons (real or virtual) allow probing the spin structure of the resonance transition. Electro-excitation allows us to map out the spatial and spin structure at varying distances by choosing the four momentum transfer to the resonance.

In these lectures, I will focus on the electromagnetic transition between non-strange baryon states. This sector received much attention in the early 1970's after the development of the first dynamical quark models. However, experimental progress was slow, partly because of the low rates associated with electromagnetic interactions, and partly because of the lack of guidance by theoretical models that went beyond the simplest quark models. It was also difficult for experiments to achieve the precision needed for a detailed analysis of the entire resonance region in terms of the fundamental photocoupling amplitudes over a large range in momentum transfer.

More realistic models were developed after the major electron accelerators used in these studies had been shut down in the wake of the J/ψ discovery in 1974. With the construction of continuous wave (CW) electron accelerators in the GeV and multi-GeV region, this situation is changing in a significant way. For example, use of large acceptance detectors at high luminosities of up to $10^{34} cm^{-2} sec^{-1}$ appears feasible, allowing measurement of several reaction channels simultaneously[6], over a large kinematic range, and with statistical accuracy comparable to that achieved with hadronic probes. Moreover, with 100% duty cycle, high statistics coincidence measurements can be conducted for exclusive channels with small cross sections. *To a large degree the statistics will not be limited by the luminosity achievable in these measurements but rather by the speed of the data acquisition system and the data analysis process.* It is interesting to note that hadronic reactions will no longer enjoy their traditional rate advantage over electromagnetic processes. This will bring to bear the full power of the electromagnetic interaction as a probe of the internal structure of hadrons and

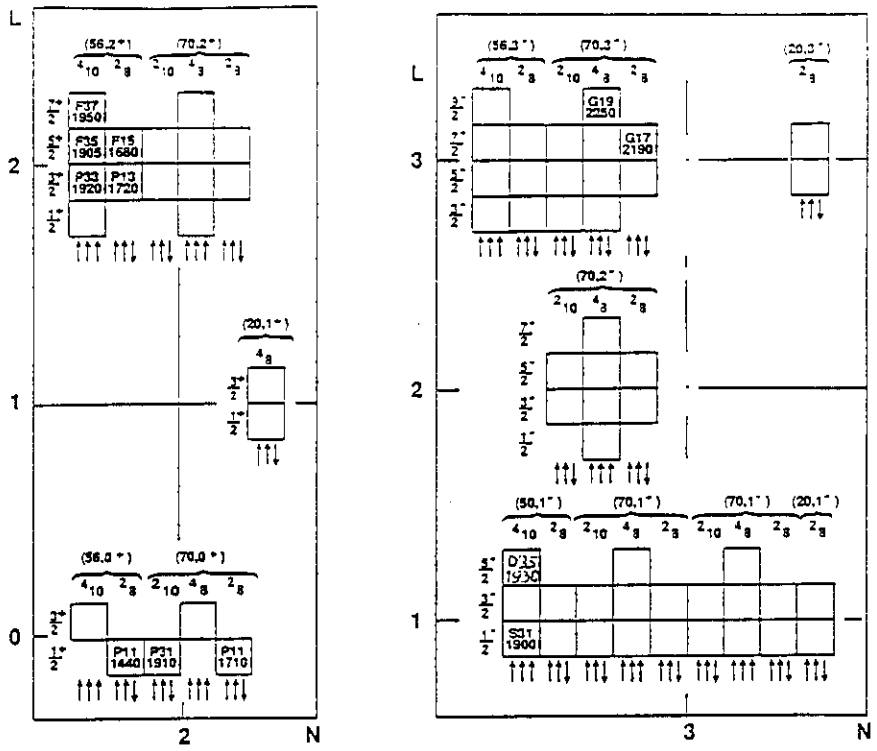

Figure 1. *Experimental status of the* $N = 2$, $L_{3q} = 1$, *and* $N = 3$, $L_{3q} = 2$, *quark model states in the* $SU(6) \otimes O(3)$ *basis.*

the strong interaction.

The lectures are organized as follows. Before reviewing the experimental status of electromagnetic transitions of baryons resonances, I will briefly discuss some aspects of baryon spectroscopy and what we have learned about the baryon structure from inclusive electron scattering in the nucleon resonance region. Then I will introduce some basic formalism which is necessary for understanding the language and analysis techniques. In the main part of this lecture I will discuss what we have learned in the past from exclusive electroproduction of low mass nucleon resonances. Finally I will discuss topics in nucleon resonance physics which are of current interest and which need to be addressed in future experiments, and outline an experimental strategy for how some of these problems may be tackled.

TOPICS IN LIGHT QUARK BARYON SPECTROSCOPY

In the course of the past decade, very little has happened in experimental light quark baryon spectroscopy, especially when considering its importance for the understanding of the structure of baryons. The field appears to be still in its infancy. The 1992 edition of the Review of Particle Properties[7] lists 19 established N^* or Δ states, and 26 candidate states with insufficient experimental evidence. This is only a small fraction of the states predicted by the most accepted QCD inspired non-relativistic constituent quark models (NRCQM). Much of the information we have on baryons states is the result of partial wave analyses of elastic pion-nucleon scattering measurements $\pi N \rightarrow \pi N$. The NRCQM allows the association of all established states with a level in the $SU(6) \otimes O(3)$ representation, where $SU(6)$ describes the symmetry

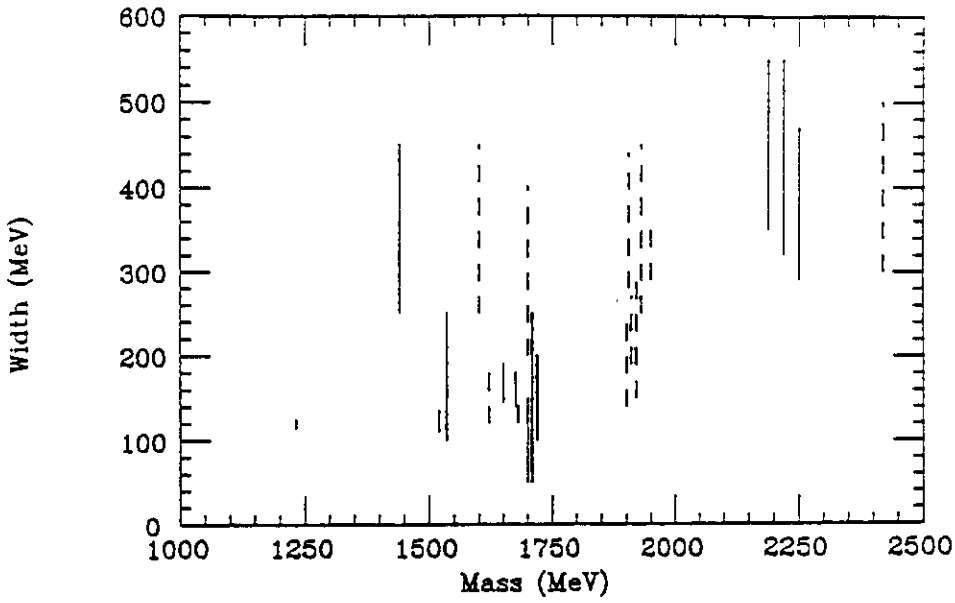

Figure 2. *Widths (including experimental uncertainties) of non-strange baryon states. Solid and dashed lines indicate isospin $\frac{1}{2}$ and $\frac{3}{2}$ states, respectively.*

properties of the spin-flavor wavefunction, and $O(3)$ is the symmetry group for the orbital angular momentum of the q^3 system. According to their symmetry properties, principal energy levels and orbital angular momentum, the 3-quark states can be associated with supermultiplets. The ground states and all states associated with the $[70, 1^-]_1$ super multiplet have been observed experimentally . However, several of the N=2 states, and most of the N=3 and N=4 states have not been seen in $\pi N \rightarrow \pi N$ reactions. Figure 1 summarizes the experimental situation for the N=2 and N=3 super multiplets.

Experimental uncertainties in the widths of many states are large (Figure 2). Even for well established states such as the $P_{11}(1440)$, the uncertainty is nearly a factor of 2. The significantly different values found for the widths of many of these states in different analyses has impact on the accuracy of the helicity amplitudes extracted in electroproduction experiments.

Missing Baryon States

It has been suggested[8] that the problem of the "missing" states in the q^3 quark model may be of experimental nature related to the lack of data in the inelastic channels. Many of the missing states are predicted to couple weakly to the πN channel due to QCD mixing effects. The $\pi N \rightarrow \pi N$ process becomes rather ineffective in searching for these states. However, many of the N=2 and N=3 states are predicted to couple strongly to $\pi\Delta$, ρN, and ω, and if the πN channel does not totally decouple from the resonance, the process $\pi N \rightarrow \pi\pi N$ may offer a better chance for detecting these states. If they decouple completely from the πN final state, the electromagnetic transitions may be the only way to search for these states.

Table 1: Decay modes of some Baryon States [%]

State	πN	ηN	$N\pi\pi$
$P_{11}(1710)$	10 - 20	20 - 40	20 - 50
$P_{13}(1720)$	10 - 20	2 - 6	≥ 35
$G_{17}(2190)$	10 - 20	1 - 3	20 - 40
$H_{19}(2220)$	10 - 20	0.5 - 1	?
$G_{19}(2250)$	5 - 15	1 - 3	?
$I_{11,1}(2600)$	5 - 10	?	?
$P_{31}(1910)$	15 - 30	-	70 - 85
$P_{33}(1920)$	5 - 20	-	?
$D_{35}(1950)$	10 - 20	-	not seen
$F_{37}(1950)$	35 - 40	-	15 - 40
$H_{3,11}(2420)$	5 - 15	-	?

Obviously, our picture of baryon structure could change dramatically if these states do not exist. An extensive search for at least some of these states is therefore important and urgent. The quark cluster model[9] and the algebraic model[4] can accommodate the known baryon spectrum, but predict a fewer number of additional states. In these models the quarks are not in a spherically symmetric configuration but rather in a diquark-quark configuration with reduced number of degrees of freedom (Figure 3). Electroproduction of nucleon resonances should be a very sensitive tool to distinguish between these alternative configurations.

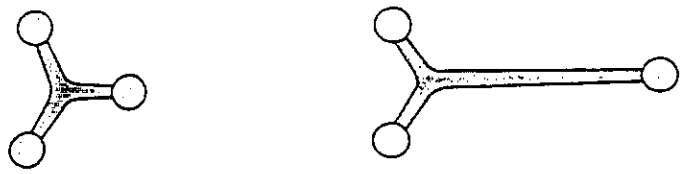

Figure 3. *Spherically symmetric q^3, and non-spherical $q^2 - q$ baryon configuration.*

Inelastic channels are not well determined experimentally, due to the lack of sufficiently detailed data in the $\pi N \rightarrow \pi\pi N$, $\pi N \rightarrow \pi\pi\pi N$, and $\pi N \rightarrow \eta N$ channels (table 1). The lack of knowledge of fundamental resonance properties has serious consequences regarding systematic uncertainties in the extraction of photocoupling amplitudes, where properties of the hadronic vertex are used as input.

Another category of baryons about which we have no experimental information is the gluonic excitations or hybrids q^3G. These states have been discussed within the framework of the bag model[10],[11]. Low lying states such as $P_{11}(1440)$, or $P_{33}(1600)$ are possible candidates for gluonic excitations. The problem is how to distinguish

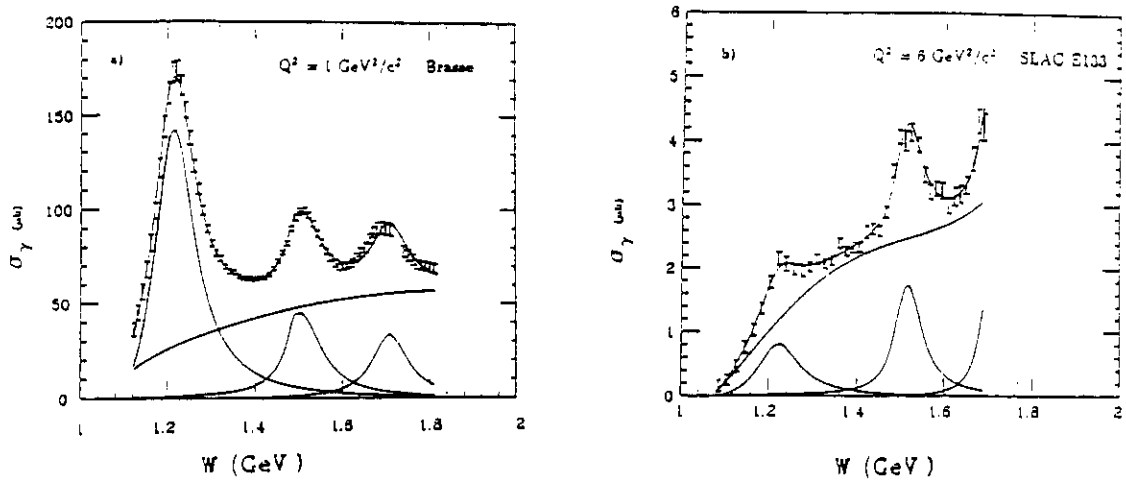

Figure 4. *The total photoabsorption cross section at various values of Q^2. Data compiled by P. Stoler*[13].

gluonic excitations from regular q^3 excitations. Some of the hybrid states, e.g. the P_{13}^G, or the P_{31}^G are not allowed in the q^3 model at these low masses, therefore their mere existence would already signal that the standard q^3 model cannot be complete. Experimental indications for these states are weak and have been found in inelastic channels only[12]. As we will discuss in lecture 3, measurements of the electromagnetic transition form factors are a powerful tool in determining the nature of these states.

INCLUSIVE ELECTRON SCATTERING

Unpolarized Electron Scattering

The inclusive electron scattering cross section $eN \rightarrow eX$ reveals a few broad bumps, clearly indicating the excitation of resonances in the mass region below 2 GeV (Figure 4). However, their broad widths and close spacing make it impossible to separate them in inclusive production reactions. Nonetheless, one can obtain some global information about the Q^2 dependence of the dominant states by subtracting the non-resonant background contribution. This technique has been used by various groups [14], most recently to study the photocoupling amplitudes of the prominent states at very high momentum transfers[13],[15]. Even without such a subtraction procedure Fig. 4 reveals that the various resonances may have very different Q^2 dependences: the first excited state, the $P_{33}(1232)$ (or $\Delta(1232)$) falls off much more rapidly with increasing Q^2 than the dominant higher mass states. A closer look shows that the position of the second and third peak are not fixed at the same mass value with varying Q^2, indicating that they are composed of several resonant states with different Q^2 dependent formfactors.

The inclusive unpolarized electron scattering cross section can be written as:

$$\frac{d\sigma}{d\Omega_e dE'_e} = \Gamma \left[\quad \right]_{TOT} \tag{1}$$

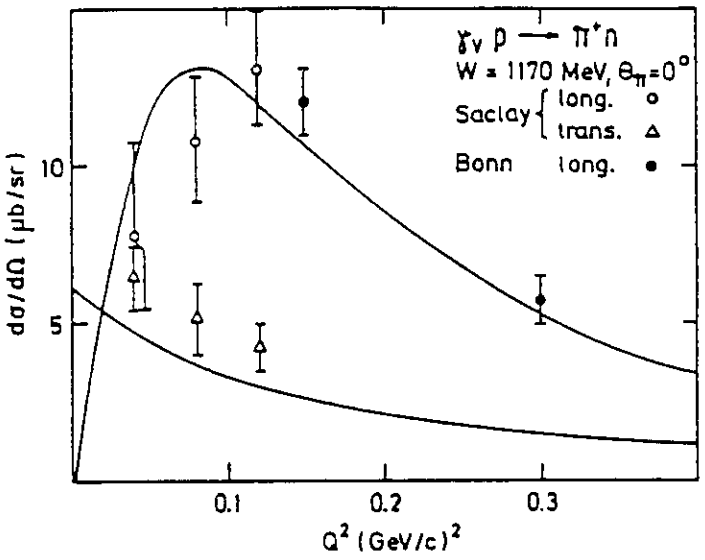

Figure 5. *σ_L and σ_T for the π^+ production off the proton below the $P_{33}(1232)$ resonance peak.*

$$\sigma_{TOT} = (\sigma_T + \epsilon\sigma_L) \quad , \tag{2}$$

where Γ_T is the virtual photon flux

$$\Gamma_T = \frac{\alpha}{4\pi Q^2} \frac{(W^2 - M^2)E'}{ME} \frac{1}{1-\epsilon}, \tag{3}$$

and ϵ describes the photon polarization. σ_T and σ_L are the transverse and longitudinal total absorption cross sections, respectively. The transverse total absorption cross section σ_T can be expressed in terms of the total absorption for helicity $\frac{1}{2}$ and helicity $\frac{3}{2}$ in the initial state photon-nucleon system:

$$\sigma_T = \frac{1}{2}(\sigma^T_{1/2} + \sigma^T_{3/2}) \quad . \tag{4}$$

σ_L contains only helicity $\frac{1}{2}$ components, and is typically small. For example, in the deep inelastic region $\sigma_L/\sigma_T \simeq 0.15$ due to the primordial transverse momentum of the quarks inside the nucleon.

In the resonance region, a significant σ_L could be evidence for non-quark degrees of freedom, such as photon absorption on spin-0 objects like pions or diquark configurations inside the nucleon. A strong longitudinal coupling to the proton is indeed observed in a kinematical regime where contributions from the pion cloud are expected to dominate: near threshold and at small values of Q^2 (Figure 5).

Quark models predict small values of σ_L/σ_T for the resonance couplings, with possible exceptions for radial excitations, such as the $P_{11}(1440)$. Accurate separate measurements of σ_L and σ_T can therefore give important global information about the internal structure of baryons.

The longitudinal part can be separated from the transverse part by measuring the ϵ dependence of the total absorption cross section. This has been done for a

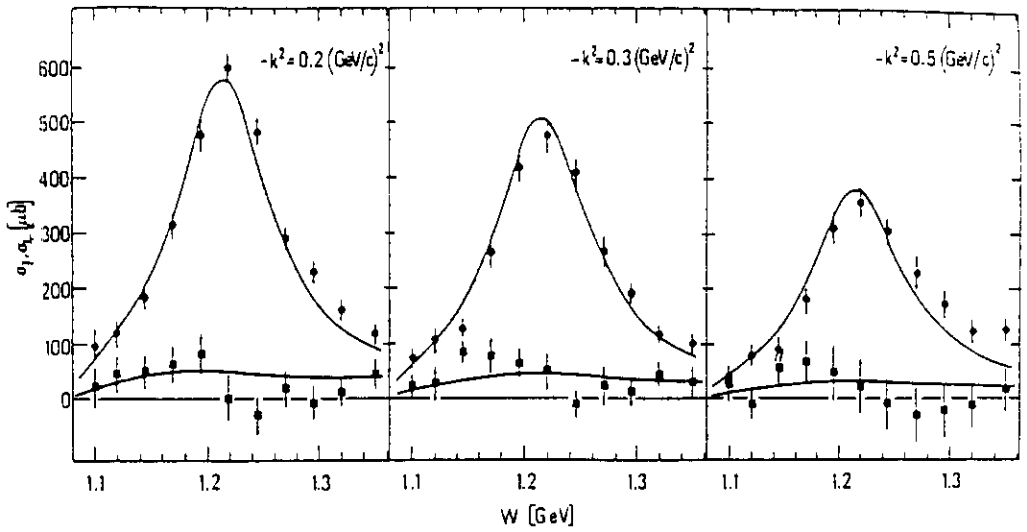

Figure 6. *Transverse and longitudinal cross section in the $P_{33}(1232)$ region ($-k^2 = Q^2$). Data from Bonn*[16].

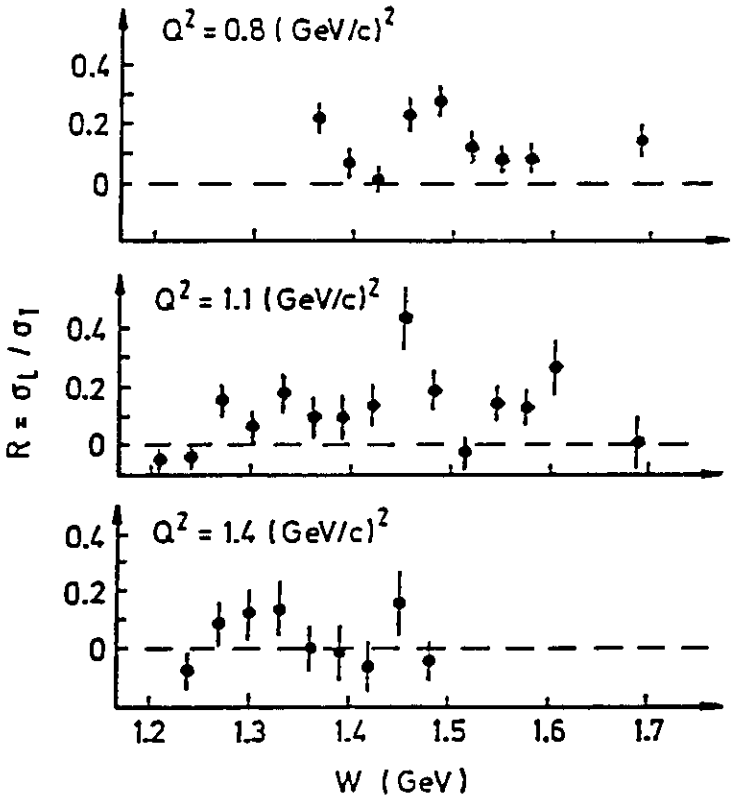

Figure 7. *Ratio σ_L/σ_T in the resonance region*[17].

few kinematical points only. The most accurate separation of σ_L and σ_T has been done at small Q^2 in the $P_{33}(1232)$ region (Figure 6), with the result that no resonant longitudinal coupling was found. Of course, the total absorption cross section is not very sensitive to relatively small amplitudes since they enter in quadrature. Therefore, small resonant longitudinal contributions are not excluded, and measurements which are more sensitive to these terms should be carried out. Results of measurements at

higher masses yield similarly small values for σ_L/σ_T (Figure 7).

In a simple analysis of the inclusive cross section one may assume an incoherent superposition of resonances and non-resonant background. At fixed Q^2

$$\sigma_{TOT}(W) = \sigma_R(W) + \sigma_{NR}(W) \ , \tag{5}$$

with a Breit-Wigner parameterization for the resonant part:

$$\sigma_R(W) = A_R \cdot \frac{\vec{Q}_R^{*2}}{\vec{Q}^{*2}} \cdot \frac{W_R^2 \cdot \Gamma \cdot \Gamma_\gamma}{(W_R^2 - W^2)^2 + \Gamma^2 W_R^2} \ , \tag{6}$$

and a polynomial for the non-resonant contribution:

$$\sigma(W) = \sqrt{W - W_{thr}} \cdot \sum_{i=0}^{m} a_i \cdot (W - W_{thr})^i \ . \tag{7}$$

Γ and Γ_γ are the total width and the radiative width, respectively. $\vec{Q}^*$ is the photon momentum in the hadronic rest frame. This expression provides an s-wave energy behaviour near threshold. The least-square fit to the data yields A_R. For the higher mass resonances A_R is a superposition of different states with different widths, and different masses. The results are therefore ambiguous, and can give only indications of the global behaviour. The $P_{33}(1232)$, however, is an isolated resonance, and the fit should yield information about the $P_{33}(1232)$ resonance only. Since σ_L is small in the $P_{33}(1232)$ region, the resonant cross section can be expressed in terms of the transverse transition form factors G_M^Δ and G_E^Δ only[28]:

$$\sigma_R \simeq \sigma_R^T = \frac{4\pi\alpha}{\Gamma} \cdot \frac{|\vec{Q}_L|^2}{W(W^2 - M^2)} \cdot (|G_M^\Delta|^2 + 3|G_E^\Delta|^2) \tag{8}$$

where $\vec{Q}_L$ is the photon momentum vector in the lab system. If G_E^Δ is small, which, as we shall see later is the case for moderate values of Q^2, one can determine $|G_M^\Delta|$. A compilation of the results from various groups is shown in Figure 8. The comparison with quark models demonstrates a longstanding problem: at the photon point, quark models underestimate the magnetic multipole transition amplitude by 20 to 30%.

Polarized Structure Functions in Inclusive Electron Scattering

If the target is polarized in the electron scattering plane the double polarized inclusive electron scattering cross section may be written as:

$$\frac{d\sigma}{d\Omega dE'} = \Gamma_T\{\sigma_T + \epsilon\sigma_L \pm \sqrt{1-\epsilon^2}\cos\psi\sigma_T A_1 \pm \sqrt{2\epsilon(1-\epsilon)}\sin\psi\sigma_T A_2\} \ , \tag{9}$$

where ψ is the polar angle of the target polarization vector relative to the photon 3-momentum vector. σ_T and σ_L are the transverse and longitudinal total photon absorption cross section, and the sign $\pm$ is related to the sign of the product of beam and target polarization (assumed to be unity). A_1 and A_2 are the polarized asymmetries:

$$A_1 = \frac{\sigma_{1/2}^T - \sigma_{3/2}^T}{\sigma_{1/2}^T + \sigma_{3/2}^T} \tag{10}$$

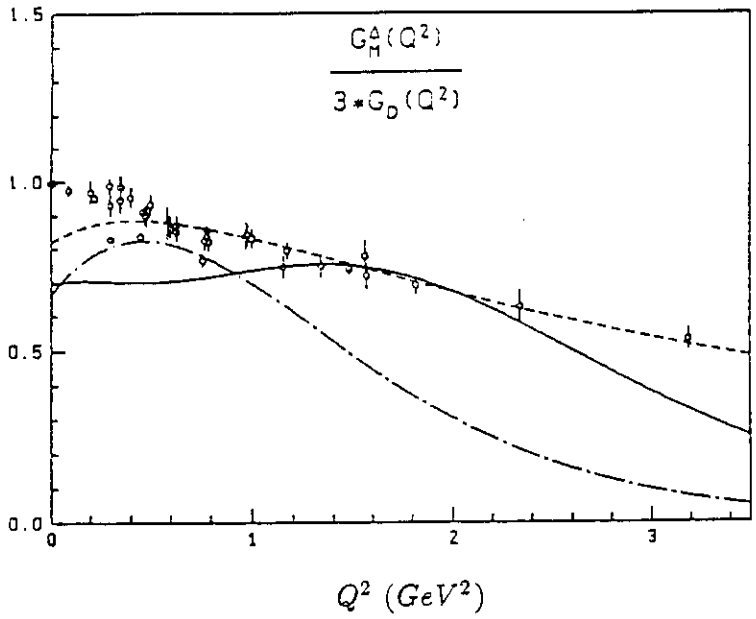

Figure 8. *The magnetic transition formfactor G_M^Δ normalized to the dipole formfactor. The curves are results of quark model calculations*[18],[19].

$$A_2 = \frac{\sigma^{TL}}{\sigma^T_{1/2} + \sigma^T_{3/2}} \quad , \tag{11}$$

where $\sigma^T_{1/2}(Q^2,\nu)$ and $\sigma^T_{3/2}(Q^2,\nu)$ are the transverse total absorption cross sections for total helicity $\lambda_{\gamma N} = \frac{1}{2}$ and $\lambda_{\gamma N} = \frac{3}{2}$, respectively. A_1 is limited to:

$$-1 \leq A_1 \leq +1 \quad .$$

A_2 is a transverse-longitudinal interference term with an upper bound of:

$$A_2 \leq \sqrt{\frac{\sigma_L}{\sigma_T}} \quad . \tag{12}$$

Since σ_L/σ_T is small throughout the resonance region, A_2 will remain relatively small too. The two polarization structure functions can be separated by polarizing the target in the scattering plane, and by varying the polarization angle ψ for fixed electron kinematics.

$A_1(W,Q^2)$ contains global information about the helicity structure of the nucleon resonances, and their Q^2 dependences. Knowledge of A_1 is also needed as an ingredient for determining the Q^2 evolution of the Gerasimov-Drell-Hearn sum rule.

An experiment at SLAC measured a combination of A_1 and A_2 (Figure 9). Although the errors are large, an interesting Q^2 dependence was revealed; the helicity asymmetry in the region of $W = 1.5-1.8\ GeV$, showed a positive value corresponding to helicity $\frac{1}{2}$ dominance at $Q^2 = 0.5\ GeV^2$, whereas at the photon point the dominant resonant states $D_{13}(1520)$ and $F_{15}(1680)$ are dominantly excited by helicity $\frac{3}{2}$. This "helicity switch" is discussed in more detail in lecture 2.

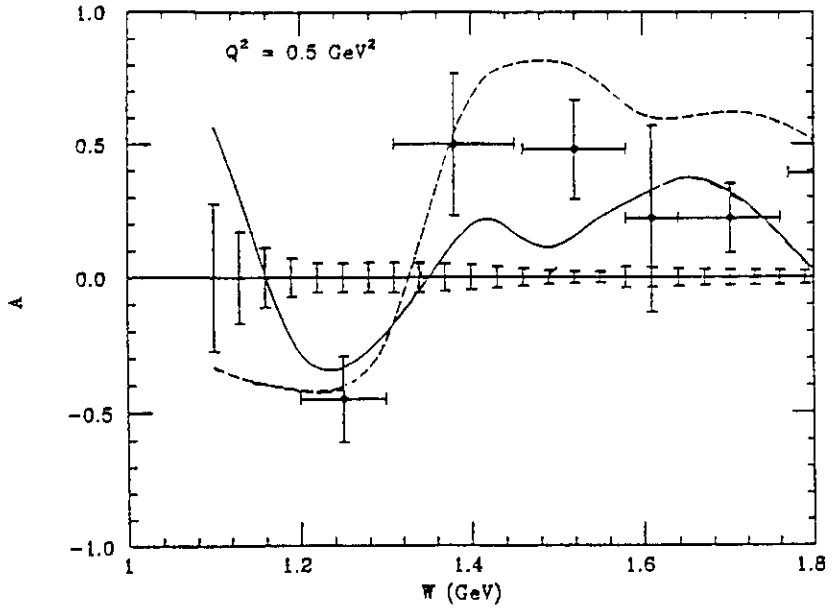

Figure 9. *Polarized inclusive structure function $A_1 + \eta A_2$ as measured at SLAC*[30]. *The bars around the horizontal axis are projected errors of an approved experiment at CEBAF.*

The asymmetry in the mass region of the $P_{33}(1232)$ remains unchanged at $\simeq -0.5$. For a magnetic dipole transition $\sigma_{1/2}/\sigma_{3/2} = \frac{1}{3}$, and therefore $A_1 = -\frac{1}{2}$, in good agreement with the data.

SINGLE PION ELECTROPRODUCTION

Inclusive measurements do not allow separation and identification of the various excited states. The three or four enhancements in the inclusive cross section correspond to about 20 excited states that may contribute for invariant masses below 2 GeV/c^2. The situation is illustrated in Figure 10. Three states may contribute to the second enhancement, and at least six states may contribute to the third bump, while even more are hidden under the rather smooth and uninteresting looking mass region around 2 GeV/c^2. As we will see later, several of the so-called "missing resonances" may be located in this mass region.

An unambiguous identification can only be accomplished by explicit measurement of the decay products such as πN, ηN, ρN, $\pi\Delta$. The $\gamma_v NN^*$ vertex for the transition into a specific state is described by two (for $J = \frac{1}{2}$ states) or three (for $J \geq \frac{3}{2}$ states) amplitudes, $A_{1/2}(Q^2)$, $A_{3/2}(Q^2)$, and $S_{1/2}(Q^2)$, where A and S refer to the transverse and scalar coupling, respectively, and the subscripts refer to the total helicity of the $\gamma_v N$ system (Figure 11). Spin and isospin can be extracted by measuring the angular distribution in different isospin channels. Many of the low lying resonances decay primarily into the πN or ηN channels. Experiments have therefore concentrated on single π and η production. In the following section our current knowledge of the resonance transition amplitudes resulting from these reactions is reviewed. Very little is known about multiple pion production processes. Some global information about the reactions $p(e, e'p\rho)$, $p(e, e'\pi\Delta)$ has been obtained from

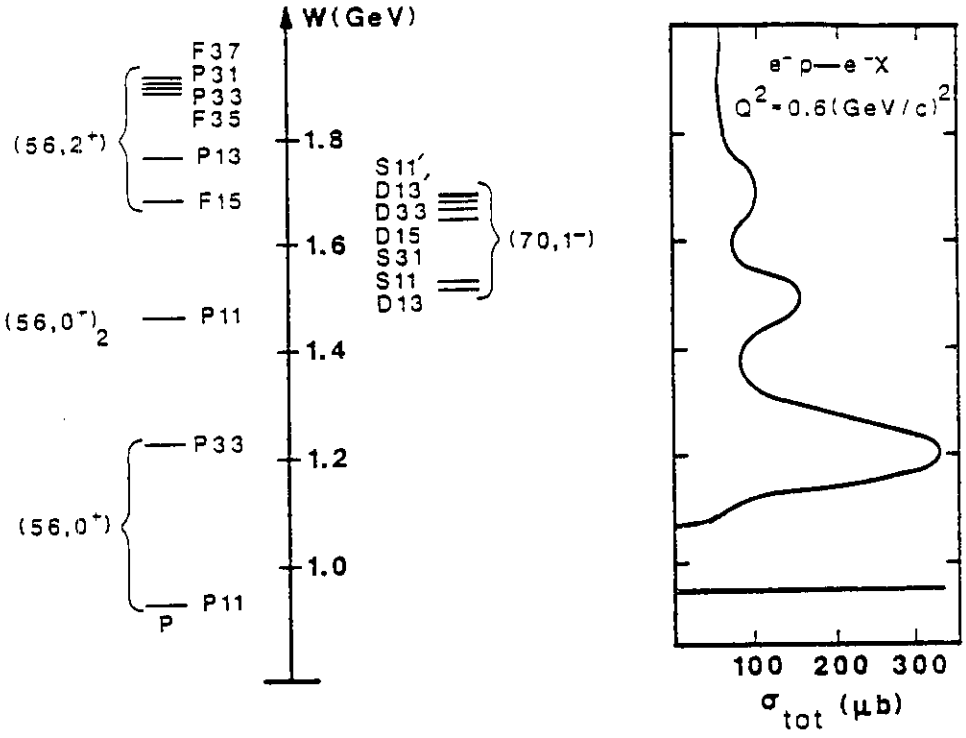

Figure 10. *The nucleon resonances with masses below 2 GeV (left) and the shape of the inclusive cross section at $Q^2 = 0.6\ GeV^2$ (right).*

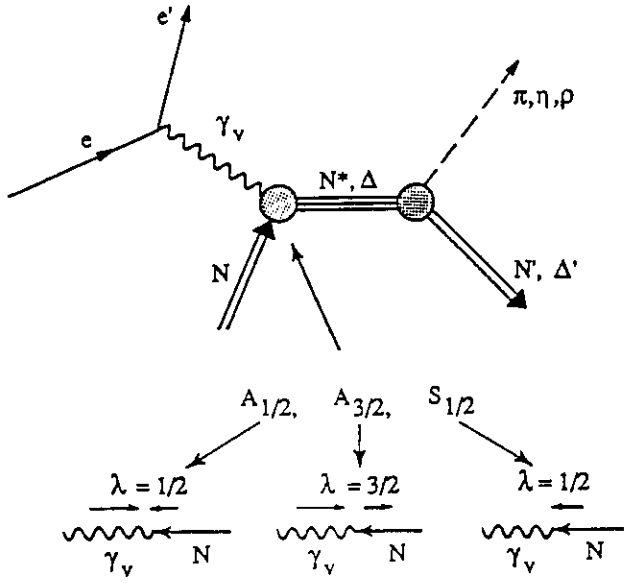

Figure 11. *Electroproduction of hadronic final states via s - channel resonance decays. The $\gamma_v NN^*$ vertex is described by the photocoupling helicity amplitudes $A_{1/2}$, $A_{3/2}$, and $S_{1/2}$, which are functions of Q^2 only.*

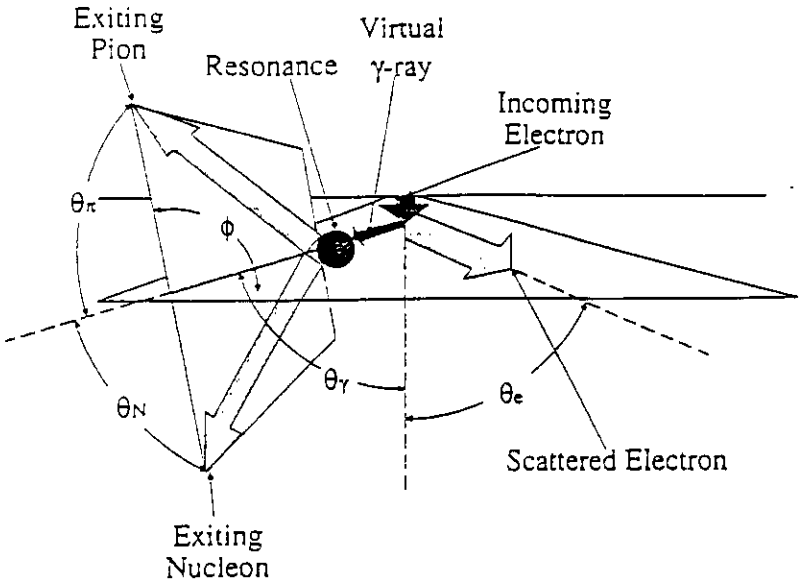

Figure 12. *Kinematics of single pion electroproduction off a nucleon.*

a DESY streamer chamber experiment[22]. However, the data are not sufficiently detailed to allow the extraction of helicity amplitudes for specific resonances.

Multipoles and Partial Wave Helicity Element

Single pion production kinematics is shown in Figure 12. The differential cross section in single meson production contains four response functions:

$$\frac{d\sigma}{d\Omega} = \sigma_T + \epsilon\sigma_L + \epsilon\sigma_{TT}\cos 2\phi + \sqrt{2\epsilon(1+\epsilon)}\sigma_{TL}\cos\phi \quad , \tag{13}$$

where ϕ is the azimuthal angle of the hadronic decay plane with respect to the electron scattering plane. The observables of the process $\gamma_v N \rightarrow \pi N$, where γ_v denotes the virtual photon, can be expressed in term of six parity conserving helicity amplitudes[26]:

$$H_i := < \lambda_\pi; \lambda_N |T| \lambda_{\gamma_v}; \lambda_p > = < 0; \pm\frac{1}{2} |T| \pm 1, 0; \pm\frac{1}{2} > \quad , \tag{14}$$

where λ denotes the helicity of the respective particle. The H_i are complex functions of Q^2, W, θ^*_π. The response functions in (13) are given by:

$$\begin{aligned}
\sigma_T &= \frac{|\vec{p}_\pi|W}{2KM} \cdot (|H_1|^2 + |H_4|^2 + |H_4|^2 + |H_4|^2) \\
\sigma_L &= \frac{|\vec{p}_\pi|W}{KM} \cdot (|H_5|^2 + |H_6|^2) \\
\sigma_{TT} &= \frac{|\vec{p}_\pi|W}{KM} \cdot Re(H_2 H_3^* - H_1 H_4^*) \\
\sigma_{TL} &= \frac{|\vec{p}_\pi|W}{\sqrt{2}KM} \cdot Re(H_5^*(H_1 - H_4) + H_6^*(H_2 + H_3)) \quad ,
\end{aligned} \tag{15}$$

where $\vec{p}_\pi$ is the pion momentum in the hadronic cms system, and K is the equivalent real photon lab energy for producing a state with mass W:

$$K = \frac{W^2 - M^2}{2M} \quad .$$

The H_i can be expanded in terms of Legendre polynomials:

$$
\begin{aligned}
H_1 &= \frac{1}{2}\sqrt{2}\sin\theta\cos\frac{\theta}{2}\sum_{l=1}^{\infty}(B_{l+}-B_{(l+1)-})(P_l''-P_{l+1}'') \\
H_2 &= \sqrt{2}\cos\frac{\theta}{2}\sum_{l=0}^{\infty}(A_{l+}-A_{(l+1)-})(P_l'-P_{l+1}') \\
H_3 &= \frac{1}{2}\sqrt{2}\sin\theta\sin\frac{\theta}{2}\sum_{l=1}^{\infty}(B_{l+}+B_{(l+1)-})(P_l''+P_{l+1}'') \\
H_4 &= \sqrt{2}\sin\frac{\theta}{2}\sum_{l=0}^{\infty}(A_{l+}+A_{(l+1)-})(P_l'+P_{l+1}') \\
H_5 &= \sqrt{2}\cos\frac{\theta}{2}\sum_{l=0}^{\infty}(C_{l+}-C_{(l+1)-})(P_l'-P_{l+1}') \\
H_6 &= \sqrt{2}\sin\frac{\theta}{2}\sum_{l=0}^{\infty}(C_{l+}+C_{(l+1)-})(P_l'+P_{l+1}') \quad ,
\end{aligned}
\tag{16}
$$

$A_{l\pm}$ and $B_{l\pm}$ are the transverse partial wave helicity elements for $\lambda_{\gamma N}=\frac{1}{2}$ and $\lambda_{\gamma N}=\frac{3}{2}$, respectively. $C_{l\pm}$ are the longitudinal partial wave helicity elements. In the subscript $l+$, and $l+1,-$ are the π (η) orbital angular momenta, and $\pm$ is related to the total angular momentum, $J=l_\pi\pm\frac{1}{2}$. The partial wave helicity elements are linear combinations of the electromagnetic multipoles:

$$
\begin{aligned}
M_{l+} &= \frac{1}{2(l+1)}(2A_{l+}-(l+2)B_{l+}) \\
E_{l+} &= \frac{1}{2(l+1)}(2A_{l+}+lB_{l+}) \\
M_{l+1,-} &= \frac{1}{2(l+1)}(2A_{l+1,-}+lB_{l+1,-}) \\
E_{l+1,-} &= \frac{1}{2(l+1)}(-2A_{l+1,-}+(l+2)B_{l+1,-}) \\
S_{l+} &= \frac{1}{l+1}\sqrt{\frac{\vec{Q}^{*2}}{Q^2}}C_{l+} \\
S_{l+1,-} &= -\frac{1}{l+1}\sqrt{\frac{\vec{Q}^{*2}}{Q^2}}C_{l+1,-} \quad ,
\end{aligned}
\tag{17}
$$

$\vec{Q}^*$ is the photon 3-momentum in the hadronic rest frame. The partial wave helicity elements contain both non-resonant and resonant contributions. An analysis must be performed to separate the resonant parts $\hat{A}_{l\pm}$, $\hat{B}_{l\pm}$, and $\hat{C}_{l\pm}$ of the amplitudes. In a final step the known hadronic properties of a given resonance can be used to determine the photocoupling helicity amplitudes which characterize the electromagnetic vertex:

$$
\begin{aligned}
\hat{A}_{l\pm} &= \mp F\cdot C^I_{\pi N}\cdot A_{1/2} \\
\hat{B}_{l\pm} &= \pm F\sqrt{\frac{16}{(2j-1)(2j+3)}}C^I_{\pi N}A_{3/2} \quad , \\
F &= \sqrt{\frac{1}{(2j+1)\pi}\frac{K}{p_\pi}\frac{M}{W_R}\frac{\Gamma_\pi}{\Gamma^2}}
\end{aligned}
\tag{18}
$$

where the $C^I_{\pi N}$ are isospin coefficients. The total absorption cross section for the transition into a specific resonance is given by:

$$\sigma_T = \frac{2M}{W_R\Gamma}(A^2_{1/2} + A^2_{3/2}) \ . \tag{19}$$

The $A_{1/2}$ and $A_{3/2}$ are the quantities often used to connect theoretical calculations to the experimental analysis. However, some models such as the Skyrme model, make direct predictions for the partial wave helicity elements[5].

Isospin Decomposition

Nucleon resonances are eigenstates of the isospin, with quantum numbers $I = \frac{1}{2}, \frac{3}{2}$. The final states in electromagnetic pion production are not eigenstates of the isospin. In order to identify the isospin of the intermediate resonant state, measurement of various channels with different isopin in the initial or final state is usually necessary. The photon transfers $\Delta I = 0, 1$ resulting in three isospin amplitudes for single pion production: T^s, T^v_1, T^v_3, where T_s is the isoscalar, T^v_1 the isovector amplitude with $I_{\pi N} = \frac{1}{2}$, and T^v_3 the isovector amplitude with $I_{\pi N} = \frac{3}{2}$. Assuming isospin symmetry, the decompositions for the various production channels are:

$$\begin{aligned}
< \pi^+ n|T|\gamma_v p > &= \sqrt{\tfrac{1}{3}}T^v_3 \ -\sqrt{\tfrac{2}{3}}(T^v_1 - T^s) \\
< \pi^0 p|T|\gamma_v p > &= \sqrt{\tfrac{2}{3}}T^v_3 \ +\sqrt{\tfrac{1}{3}}(T^v_1 - T^s) \\
< \pi^- p|T|\gamma_v n > &= \sqrt{\tfrac{1}{3}}T^v_3 \ -\sqrt{\tfrac{2}{3}}(T^v_1 + T^s) \\
< \pi^0 n|T|\gamma_v n > &= \sqrt{\tfrac{2}{3}}T^v_3 \ +\sqrt{\tfrac{1}{3}}(T^v_1 + T^s)
\end{aligned}$$

Note that because of the differences in the masses of charged and neutral pions and nucleons, isospin symmetry is broken near pion threshold. Production of η and ω mesons selects directly $I = \frac{1}{2}$ contributions and allows isolation of the N^* resonances.

The Transition γ_v p $\rightarrow$ $P_{33}(1232)$.

In $SU(6)$ symmetric quark models, this transition is described by a simple quark spin-flip in the $L_{3Q} = 0$ ground state, corresponding to a magnetic dipole transition M_{1+}. The electric and scalar quadrupole transitions are predicted to be:

$$E_{1+} = S_{1+} \equiv 0 \ . \tag{20}$$

In more elaborate QCD based models which include color magnetic interactions arising from the one-gluon exchange at small distances, the $P_{33}(1232)$ acquires an $L_{3Q} = 2$ component. This leads to small electric and scalar contributions. Dynamical quark model calculations predict E_{1+}/M_{1+} to remain small (≤ 0.1) over a large Q^2 range, and to have a weak dependence on Q^2. At very high Q^2, helicity conservation requires[15] $E_{1+}/M_{1+} \rightarrow 1$, and $S_{1+}/M_{1+} \rightarrow 0$. Precise measurements of these contributions from $Q^2 = 0$ to very large Q^2 are obviously important for the development of realistic models of the nucleon.

In the region of the $P_{33}(1232)$, one may expect that only s- and p- waves with $J \leq \frac{3}{2}$ contribute. In this approximation, the partial wave expansion in the differential

cross section leads to:

$$\frac{d\sigma}{d\Omega} = A_0 + \epsilon B_0 + \cos\theta(A_1 + \epsilon B_1) - \cos^2\theta(A_2 + \epsilon B_2) + \epsilon C_2 \sin^2\theta \cos 2\phi + \sqrt{\epsilon(1+\epsilon)} \sin\theta \cos\theta(D_0 + D_1 \cos\theta). \quad (21)$$

which contains nine measurable quantities $A_0, B_0, A_1, \ldots$. The unknown multipoles in this approximation are: E_{0+}, M_{1-}, E_{1+}, M_{1-}, S_{0+}, S_{1-}, S_{1+}. Since the multipoles are complex quantities there are 14 unknown numbers, which cannot be determined unambiguously from the partial wave expansion coefficient without further assumptions. In the region of the $P_{33}(1232)$ the process $\gamma_v p \rightarrow \pi^0 p$ is dominated by a M_{1+} magnetic dipole transition. Therefore retaining only terms containing the M_{1+} may be a reasonable approximation near the resonance peak. The cross section then reduces to:

$$\begin{aligned}\frac{d\sigma}{d\Omega} \simeq & \frac{|\vec{p}_\pi W|}{KM} \cdot \Big[\frac{5}{2}|M_{1+}|^2 - 3Re(M_{1+}E_{1+}^*) + Re(M_{1+}M_{1-}^*) \\ & + 2\cos\theta Re(E_{0+}M_{1+}^*) \\ & + \cos^2\theta\Big(-\frac{3}{2}|M_{1+}|^2 + 9Re(M_{1+}E_{1+}^*) - 3Re(M_{1-}M_{1+}^*)\Big) \\ & + \epsilon\sin^2\theta\cos 2\phi\Big(-\frac{3}{2}|M_{1+}|^2 - 3Re(M_{1+}E_{1+}^*)\Big) \\ & - \sqrt{2\epsilon_L(\epsilon+1)}\sin\theta\cos\phi\big(Re(S_{0+}M_{1+}^*) + 6\cos\theta Re(S_{1+}M_{1+}^*)\big)\Big] \quad , \end{aligned} \quad (22)$$

where θ is the pion cms polar angle, and $\epsilon_L = Q^2/\vec{Q}^{*2}\epsilon$. The sensitivity to the electric and scalar quadrupole transitions rests with the interference terms of E_{1+} and S_{1+} with M_{1+}.

In this approximation the resonant terms

$$|M_{1+}|, \; Re(M_{1+}E_{1+}^*), \; Re(M_{1+}S_{1+}^*)$$

and the non-resonant terms

$$Re(E_{0+}M_{1+}^*), \; Re(S_{0+}M_{1+}^*), \text{ and } Re(M_{1-}M_{1+}^*)$$

can be determined unambiguously by measuring the ϕ and θ dependence of the differential cross section. Figure 13 shows the result of such an analysis.

Experimental data on $Re(E_{1+}M_{1+}^*)/|M_{1+}|^2$ and $Re(S_{1+}M_{1+}^*)/|M_{1+}|^2$ at the $P_{33}(1232)$ resonance mass are shown in Figure 14 and 15, respectively. The results confirm that the ratio E_{1+}/M_{1+} at the resonance mass is quite small, in qualitative agreement with $SU(6)$ and CQM predictions. However, the quality of the data is clearly not sufficient to discriminate against any of the models. For the ratio $Re(S_{1+}M_{1+}^*)/|M_{1+}|^2$ there seems to be a discrepancy with the quark model predictions. However, a warning may be in order here: The data in Figure 14 and 15 have not been analyzed to isolate the resonant contributions. They may therefore contain significant non-resonant contributions, whereas the model predictions are for the resonant parts only.

Experiments are in preparation[24, 25] to measure the quadrupole transitions over a large Q^2 range, using polarized electron beams and/or recoil polarimeters. In these experiments one obtains information not only about the terms

$$M_{1+}, \; Re(E_{1+}M_{1+}^*), \; Re(S_{1+}M_{1+}^*)$$

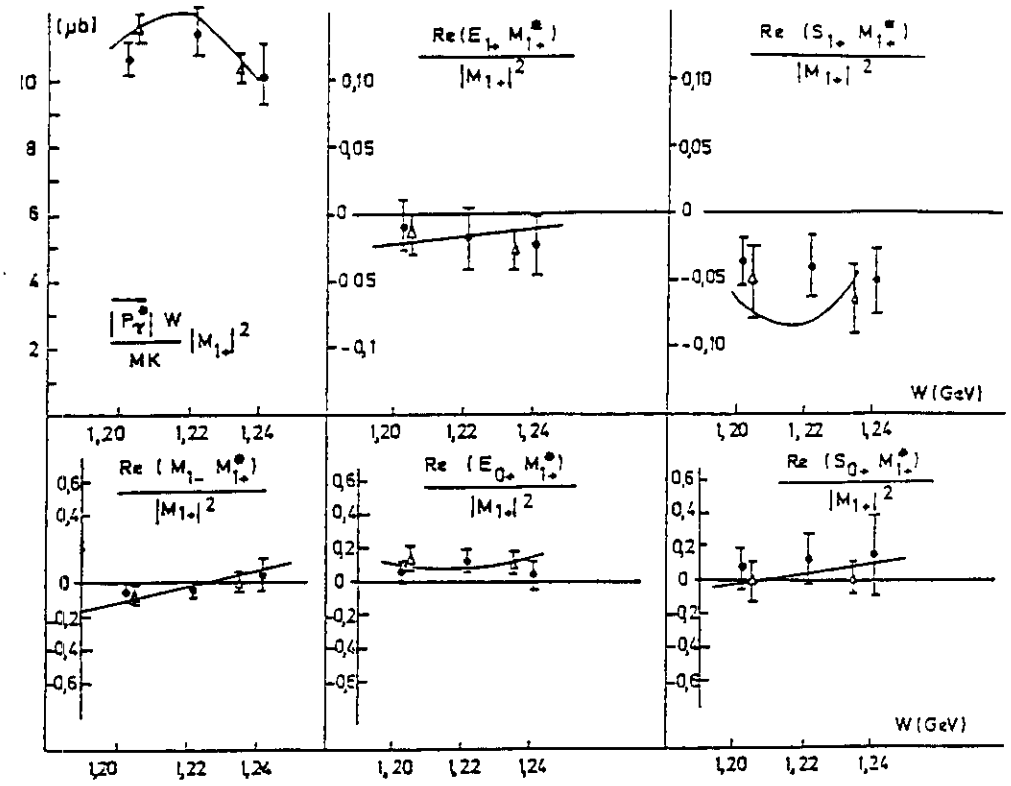

Figure 13. *Multipole analysis of $\gamma_v p \to \pi^0 p$ in the $P_{33}(1232)$ region. Data from Bonn*[23].

but also about the corresponding imaginary parts:

$$Im(E_{1+}M_{1+}^{*}) \ , \ Im(S_{1+}M_{1+}^{*}).$$

The imaginary parts of the bilinear terms can be measured only by using polarization degrees of freedom. They are particularly sensitive to phase relations between the multipoles. If the multipoles were strictly in phase, these terms would vanish identically.

Phenomenological Analysis of Pion Production.

For the analysis of the resonance region at masses up to 1.8 GeV, the procedure described for the $P_{33}(1232)$ to directly extract the multipoles is not feasible any more as one has to include partial waves up to at least $l_\pi = 3$, and $J \leq 5/2$, and unlike in the $\Delta(1332)$ region there is not a single resonant amplitude that completely dominates the differential cross section. Moreover, resonances become broader and overlap, and interferences between resonant amplitudes and between resonant and non-resonant amplitudes become increasingly important. Therefore, alternative analysis methods have been developed that take into account all resonant amplitudes. In addition, a theory or a phenomenological model for the non-resonant amplitudes is needed. To cope with the limited volume of electroproduction data it has been necessary to also make assumptions about the energy dependence of the resonant amplitudes. In photoproduction where sufficient data are available energy-independent analyses have been performed. Two different methods have been employed in electroproduction,

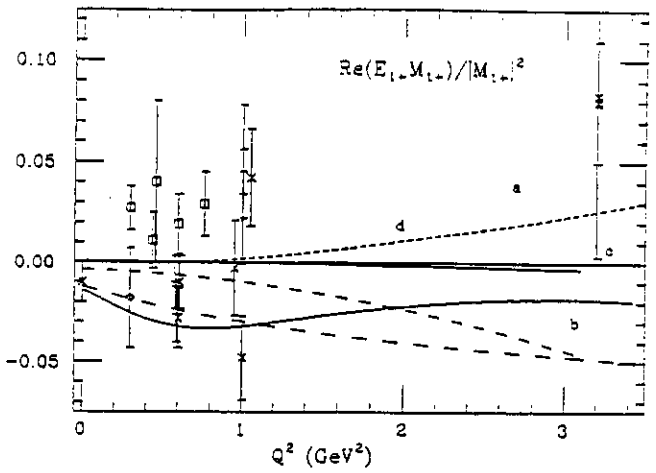

Figure 14. *Ratio* $Re(E_{1+}M_{1+}^{*})/|M_{1+}|^2$ *from electroproduction experiments*[65].

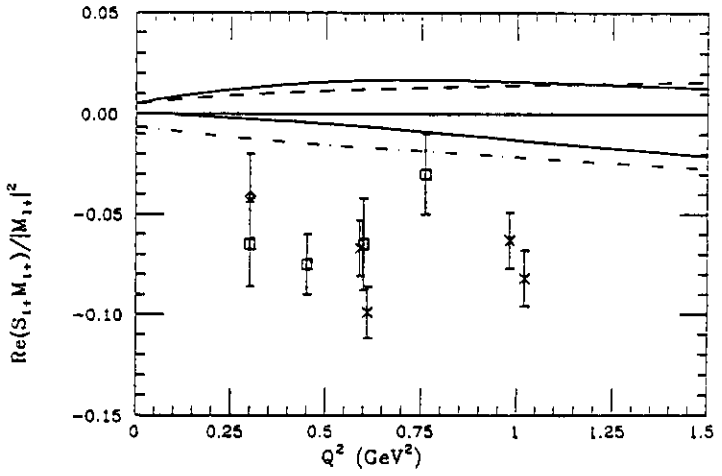

Figure 15. *Ratio* $Re(S_{1+}M_{1+}^{*})/|M_{1+}|^2$ *from electroproduction experiments*[65].

the isobar analysis method, and the dispersion relation method at fixed momentum transfer t.

Isobar analysis

In the isobar analysis[26] it is assumed that (1) the resonance masses, spin, isospin, and hadronic decay widths are known from πN scattering analysis, (2) that the nature of the energy dependence of the resonant part is known, and that it e.g. can be described by relativistic Breit-Wigner amplitudes, (3) that pion production can be described by resonant s-channel amplitudes, real Born amplitudes, and additional real background amplitudes with reasonable threshold and high energy behaviour. Obviously, this method will give results that to some degree depend on the specific assumptions about the non-resonant amplitudes. The method works well if resonances constitute the dominant part of the amplitudes, which is largely the case in single pion photo- or electroproduction for masses up to about 1.7 GeV.

Fixed-t dispersion relation analysis

The application of dispersion relations[27],[28] is based on the observation that

phenomenological analysis of pion photoproduction data yield good fits assuming real background amplitudes. This suggests that resonances approximately saturate the imaginary parts of the amplitudes, and the real and imaginary parts are related by dispersion relations:

$$Re A_i(s,t) = B_i(s,t) + \int_{(M+m_\pi)^2}^{+\infty} ds' \left[\frac{Im A_i(s',t)}{s-s'} \pm \frac{Im A_i(s',t)}{s'-u} \right] \quad . \qquad (23)$$

B_i are the Born amplitudes, and $Im A_i$ are the imaginary parts of the resonant amplitudes. The advantage of this method is that it implements all general principles such as unitarity, analyticity, crossing symmetry. On the other hand, assumptions about the high energy behavior of the imaginary parts of the invariant amplitudes are necessary, and since integration is performed into the unphysical region questions about the convergence of the multipole series at $|\cos\theta| \geq 1$ remain. In the analysis of pion photoproduction data, this method has been used very successfully. In pion electroproduction, good fits have been obtained for $Q^2 \leq 2\ GeV^2$ (Figure 16).

A realistic analysis must also take into account effects resulting from the opening up of channels other that single pion production. These so-called cusp effects are the result of unitarity constraints on the amplitudes. That these effects can be quite significant is illustrated in Figure 17, which clearly shows the influence of the η threshold on the $\pi^0 p$ and $\pi^+ n$ channels. The very different effect on the charged and neutral pion channels is explained by the larger non-resonant contributions (real part of amplitude) in the $\pi^+ n$ channel while $\pi^0 p$ is dominated by resonant contributions (imaginary part of amplitude). Similar effects are expected to arise from other channels such as $\Delta\pi$.

In the following section I will discuss results of analyses of electroproduction data in terms of resonance couplings.

Electromagnetic Transitions to the $[70,1^-]_1$ and $[56,2^+]_2$

Of the seven non-strange states associated with the $[70,1^-]_1$ supermultiplet only the $D_{13}(1520)$ and the $S_{11}(1535)$ have been studied in electroproduction experiments in some detail.

The $S_{11}(1535)$ Resonance

The $S_{11}(1535)$ is characterized by a large branching ratio into the ηN channel ($\approx 50\%$). Since the nearby $D_{13}(1520)$ state has a very small decay width into ηN, the $S_{11}(1535)$ can be separated by measuring the differential cross section $ep \rightarrow e'p\eta$. This process is dominated by resonant s - wave contributions. The angular distribution is isotropic, consistent with an s-wave behavior, and the energy dependence is dominated by resonance behavior (Figure 18).

For s-wave dominance the differential cross section can be written as:

$$\frac{d\sigma}{d\Omega_\eta^*} = A(W,Q^2) + \epsilon B(W,Q^2)$$

$$A = \frac{|\vec{p}_\eta^*|W}{MK} |A_{0-}|^2 \qquad (24)$$

$$B = \frac{|\vec{p}_\eta^*|W}{MK} \frac{Q_0^2}{\vec{Q}^{*2}} |C_{0+}|^2$$

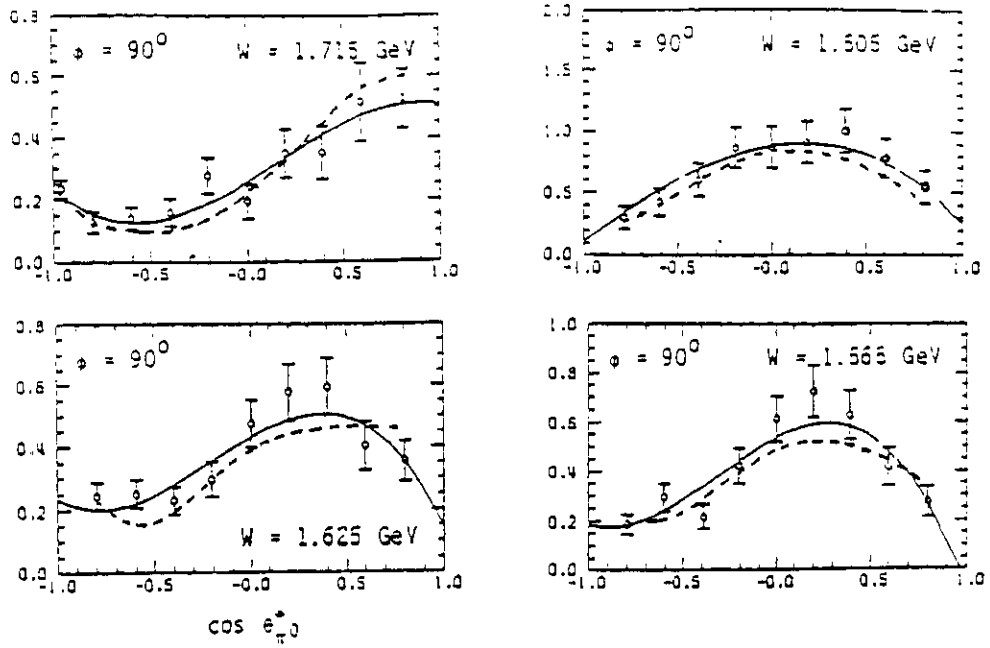

Figure 16. *Example of a dispersion fit (dashed lines) to electroproduction data in the region of the second resonance at $Q^2 = 2\ GeV^2$. The solid lines represent the results of a partial wave analysis fit*[29].

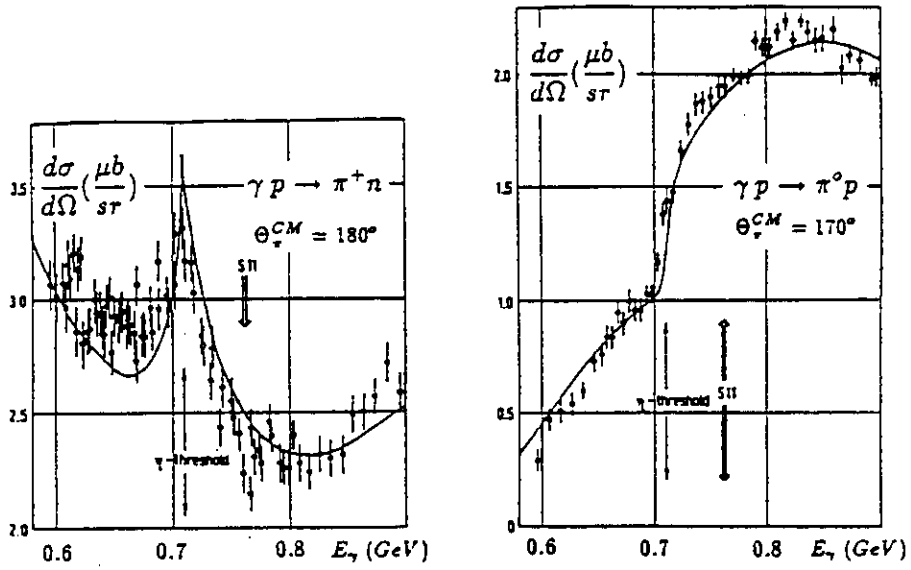

Figure 17. *Differential cross section $\gamma p \to \pi^+ n$ and $\gamma p \to \pi^0 p$ at the η threshold*[30].

For $Q^2 \leq 1\ GeV^2$, the transverse and the longitudinal contributions have been measured using Rosenbluth separation (Figure 19).

The transverse photocoupling amplitude can then be determined (Figure 20). It shows an unusually slow falloff with Q^2 which cannot be explained in the simple NRCQM. However, recent extensions of the model to include relativistic effects have been more successful in approximately reproducing this behavior. It is interesting to note that within the framework of a specific model, the absolute normalization and the Q^2 dependence appear to be sensitive to the parameterization of the confinement potential. This lends credibility to the idea that a great deal can be learned about the properties of the confinement potential by carefully studying many resonance transitions.

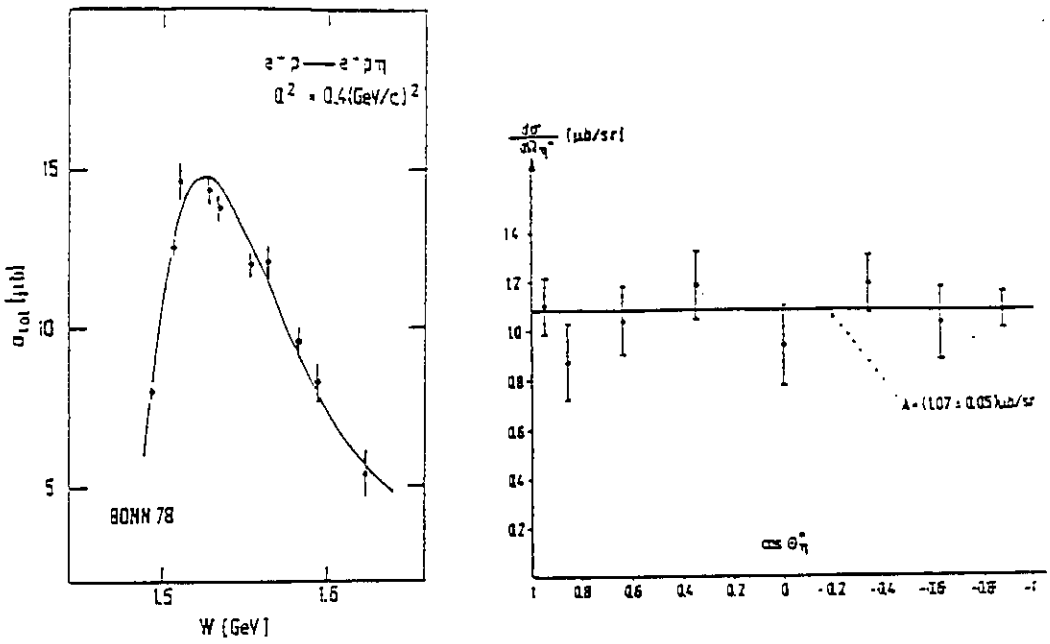

Figure 18. *Energy and angular dependence of η electroproduction* [31],[32].

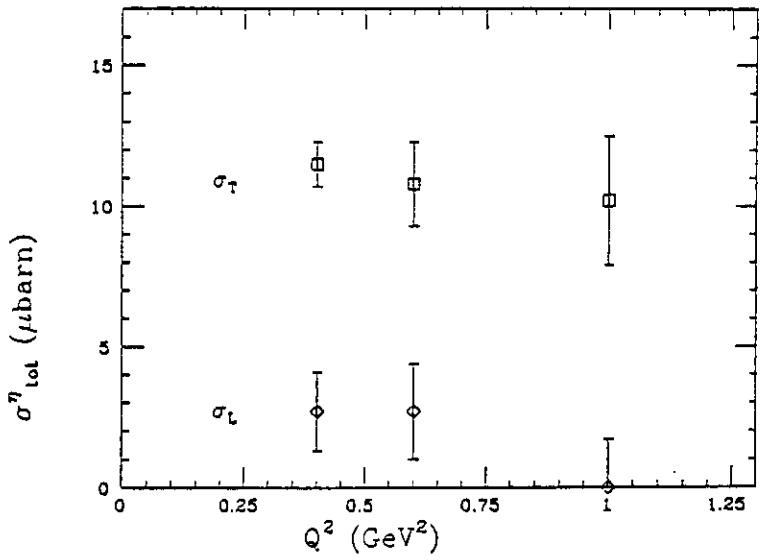

Figure 19. *Transverse and longitudinal photoabsorption cross section for $\gamma_v p \to \eta p$ at the $S_{11}(1535)$ resonance.*

Helicity structure of the $D_{13}(1520)$ and the $F_{15}(1680)$

In photoproduction the $D_{13}(1520)$ and the $F_{15}(1680)$ are both excited predominantly by $A_{3/2}$ transitions. This behavior can be accommodated in the harmonic oscillator NRCQM. In this model[37] only single quark spin-flip and single quark orbit-flip amplitudes occur. The ratio of the helicity amplitudes in this model is:

$$\frac{A^{D13}_{1/2}}{A^{D13}_{3/2}} = \frac{1}{\sqrt{3}}\left(\frac{\vec{Q}^2}{\alpha^2} - 1\right) \tag{25}$$

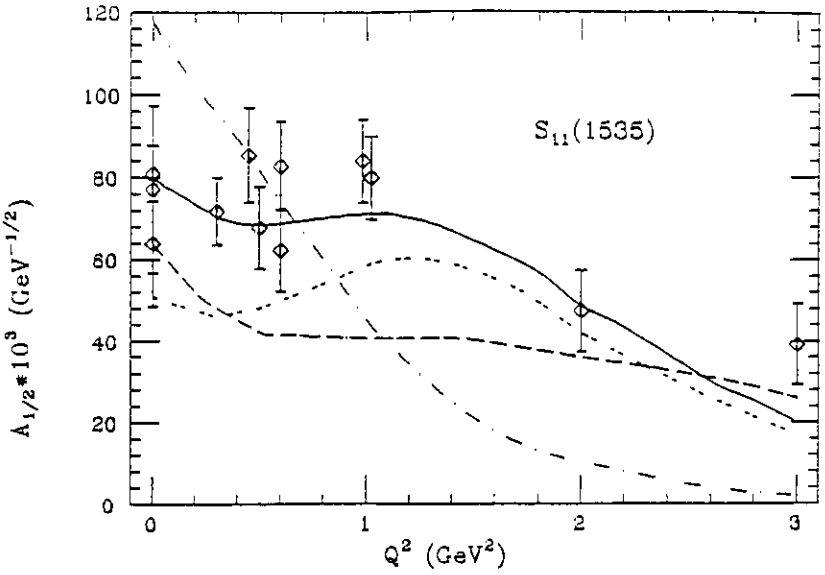

Figure 20. *Transverse amplitude $A_{1/2}$ for the transition $\gamma_v p S_{11}(1535)$. Model calculations by Close and Li[33] (short dashes), Warns et al[18] (solid line, double-dashed line for different confinement potentials), Foster and Hughes[19] (dots), Konen and Weber[34] (long dashes), Forsyth and Babcock [35] (dashed-dotted).*

$$\frac{A_{1/2}^{F15}}{A_{3/2}^{F15}} = -\frac{1}{2\sqrt{2}}\left(\frac{\vec{Q}^2}{\alpha^2} - 2\right) \quad , \tag{26}$$

where the $\vec{Q}^2$ dependent term comes from the spin-flip, and the constant term from the orbit-flip contribution. The ratios can be made to disappear by requiring $\alpha^2 \simeq \vec{Q}^2$ for the $D_{13}(1520)$ and $\alpha^2 \simeq \vec{Q}^2/2$ for the $F_{15}(1680)$, which can be accommodated simultaneously with $\alpha^2 = 0.17\ GeV^2$ for $\vec{Q}^2$ in the lab frame. With increasing Q^2, $A_{1/2}$ is then predicted to become the dominant contribution in either case[38]. Relativized versions of the NRCQM predict qualitatively the same behavior. This may be best demonstrated by displaying the helicity asymmetry

$$A_{\frac{1}{2},\frac{3}{2}} = \frac{A_{1/2}^2 - A_{3/2}^2}{A_{1/2}^2 + A_{3/2}^2} \quad .$$

A compilation of the data[39],[40] is presented in Figure 21 and Figure 24. It is worth noting that effects due to the spatial wave function tend to cancel out in this quantity. The helicity asymmetry is therefore sensitive to the spin-flavor wavefunction. The helicity switch agrees qualitatively with quark model predictions. Calculations for neutron targets show different sensitivity to ingredients of the model. Excitation of neutron resonances provides independent information about the nucleon structure.

Test of the Single Quark Transition Model

To the degree resonance transitions can be described by a single quark transitions in $SU(6)_W$ symmetric models, radiative transitions between the $[56, 0^+]_0$ and the $[70, 1^-]_1$ multiplet are completely determined by three amplitudes[41], usually called A, B, and C, where A is related to the quark orbit flip current, B to the spin flip current, and C to the combined spin-orbit flip current with $\Delta L_z = 1$. In the SQTM

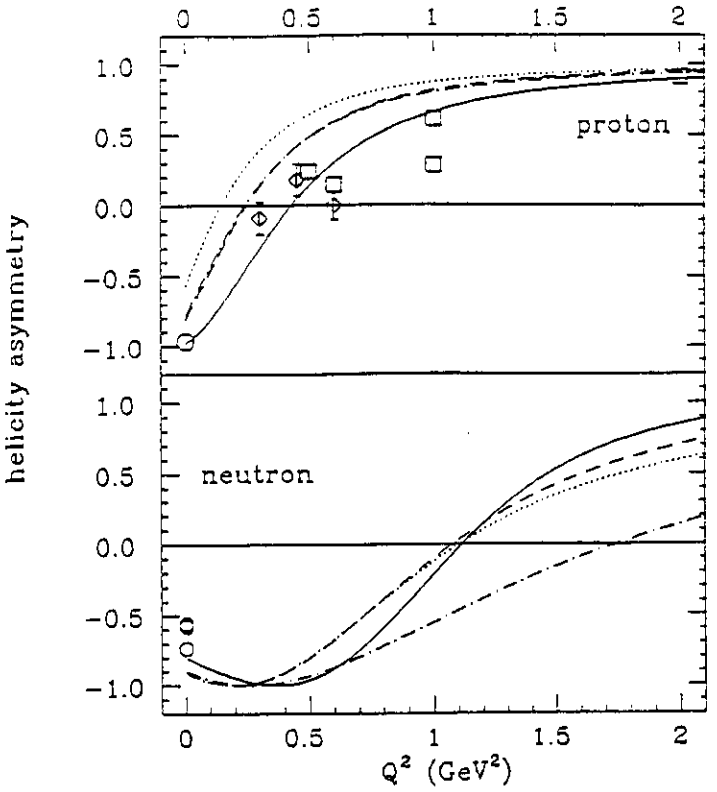

Figure 21. *Helicity asymmetry of the $\gamma_v p D_{13}(1520)$ transition. Quark-model calculations by Capstick[3] with different corrections to the NRCQM.*

radiative transitions between all states belonging to these multiplets can be expressed in terms of linear combinations of these amplitudes (table 2).

Using the known $A_{1/2}$, $A_{3/2}$ amplitudes for the $S_{11}(1535)$ and the $D_{13}(1520)$ the A, B, C amplitudes can be determined (Figure 22). There is clear evidence for the existence of a non-zero spin-orbit flip amplitude C, which does not exist in the simple NRCQM. The SQT amplitudes can be used to predict transition amplitudes for other states in the same supermultiplet. Unfortunately, information from other states is limited to proton targets and is of poor quality. Current experimental information of the $S_{11}(1650)$, $S_{31}(1620)$, and $D_{33}(1700)$ is summarized in Figure 23. With the possible exception of the $S_{31}(1620)$, the data are not in disagreement with the SQTM predictions, however, they are not accurate enough to test deviations from the SQTM. Whether the deviations seen for the $S_{31}(1620)$ at small Q^2 are significant remains to be seen when more accurate and more complete data will be available.

The most prominent state in $[56, 2^+]_2$ is the $F_{15}(1688)$, and it is the only one that has been studied experimentally over an extended Q^2 range. Similar to the $D^+_{13}(1520)$, the photoexcitation is dominantly helicity 3/2 and $A^+_{1/2}(F_{15}) \approx 0$, at $Q^2 = 0$. The data show a rapid change in the helicity structure with rising Q^2 (Figure 24). The switch to helicity 1/2 dominance is qualitatively reproduced by quark model calculations. However, much improved data are needed for a more definite comparison with the theory.

In the SQTM the transition to the $[56, 2^+]_2$ can be described by four amplitudes A′, B′, C′,and D′. D′ is a spin-orbit flip amplitude with $\Delta L_z = 2$. Without additional assumptions the four contributing SQTM amplitudes cannot presently be determined from available data due to the lack of electroproduction data for a second state in the $[56, 2^+]_2$. The $F_{37}(1950)$ would be a good candidate to obtain additional information

Table 2: Single Quark Transition Amplitudes for $\gamma + [56, 0^+]_0 \rightarrow [70, 1^-]_1$

State	Proton Target	Neutron Target
$S_{11}(1535)$:	$A^+_{\frac{1}{2}} = \frac{1}{6}(A + B - C)cos\theta$ *	$A^o_{\frac{1}{2}} = -\frac{1}{6}(A + \frac{1}{3}B - \frac{1}{3}C)$
$D_{13}(1520)$:	$A^+_{\frac{1}{2}} = \frac{1}{6\sqrt{2}}(A - 2B - C)$, $A^+_{\frac{3}{2}} = \frac{1}{2\sqrt{6}}(A + C)$	$A^o_{\frac{1}{2}} = -\frac{1}{18\sqrt{2}}(3A - 2B - C)$ $A^o_{\frac{3}{2}} = \frac{1}{6\sqrt{6}}(3A - C)$
$S_{11}(1650)$:	$A^+_{\frac{1}{2}} = \frac{1}{6}(A + B - C)\sin\theta$	$A^o_{\frac{1}{2}} = \frac{1}{18}(B - C)$
$D_{13}(1700)$:	$A^+_{\frac{1}{2}} = A^+_{\frac{3}{2}} = 0$	$A^o_{\frac{1}{2}} = \frac{1}{18\sqrt{5}}(B - 4C)$ $A^o_{\frac{3}{2}} = \frac{1}{6\sqrt{15}}(3B - 2C)$
$D_{15}(1670)$:	$A^+_{\frac{1}{2}} = A^+_{\frac{3}{2}} = 0$	$A^o_{\frac{1}{2}} = -\frac{1}{6\sqrt{5}}(B + C)$ $A^o_{\frac{3}{2}} = -\frac{1}{6}\sqrt{\frac{2}{5}}(B + C)$
$D_{33}(1670)$:	$A^+_{\frac{1}{2}} = \frac{1}{18\sqrt{2}}(3A + 2B + C)$ $A^+_{\frac{3}{2}} = \frac{1}{6\sqrt{6}}(3A - C)$	same same
$S_{31}(1650)$:	$A^+_{\frac{1}{2}} = \frac{1}{18}(3A - B + C)$	same

* (θ = mixing angle between $^4[8]_{1/2}$ and $^2[8]_{1/2}$ in $\{70, 1^-\}_1$)

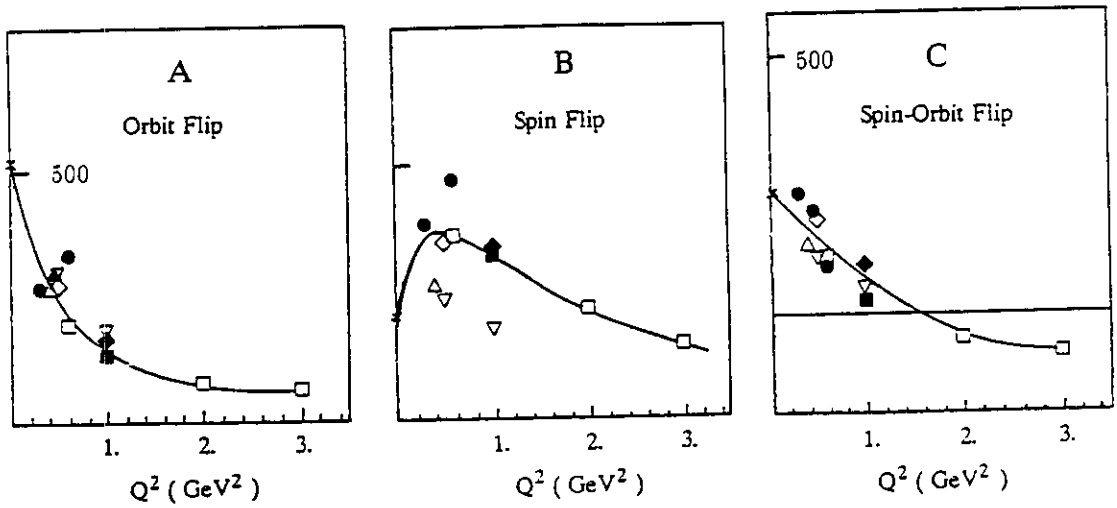

Figure 22. *Single quark transition amplitudes A, B, C in units* $10^{-3}\ GeV^{-1/2}$

as it has a large decay width into the πN channel and can be studied in single pion production.

TOPICS IN NUCLEON RESONANCE PHYSICS

In this section I want to discuss some problems that have generated a great deal of interest in recent years. Their resolution may have a significant impact on our

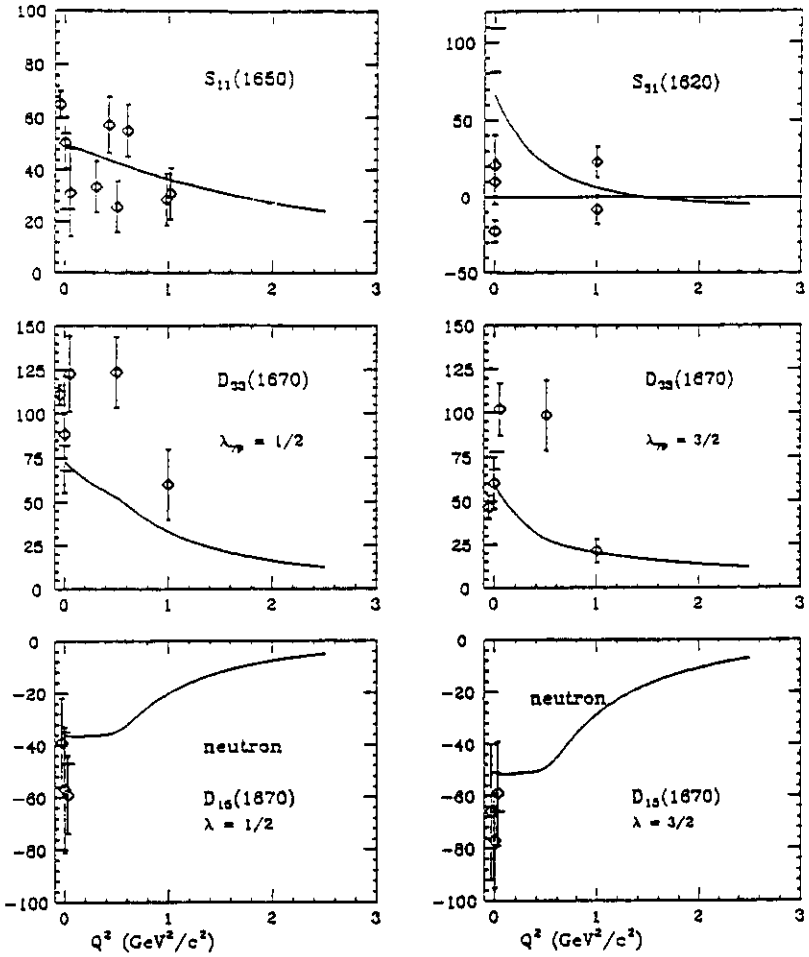

Figure 23. *Transverse photocoupling amplitudes for the the* $S_{11}(1650)$, $S_{31}(1620)$, *and* $D_{33}(1700)$ *states. The curves represent SQTM predictions using* $S_{11}(1535)$ *and* $D_{13}(1520)$ *data and the algebraic relations of Hey and Weyers*[41]. *A mixing angle between the* $[^4 8]$ *and* $[^2 8]$ *quark model states in* $[70, 1^-]$ *of* $\theta = 38^o$ *was used.*

understanding of baryon structure. These issues have either not been addressed at all, or have not been addressed adequately in previous experiments.

Electroquenching of the $P_{11}(1440)$

In the NRCQM the lowest mass $P_{11}(1440)$ state is assigned to a radially excited q^3 state within the $SU(6) \otimes O(3)$ super-multiplet $[56, 0^+]_2$ (i.e. $L_{3Q} = 0$, $N_{3Q} = 2$). However, the observed low mass of the state, as well as the sign and magnitude of the photocoupling amplitudes have traditionally been difficult to reproduce within the framework of the NRCQM. Moreover, there is experimental evidence that the Q^2 dependence of the photocoupling amplitude $A_{1/2}(Q^2)$ is quite different from what is predicted in the framework of the NRCQM. The data indicate a rapid fall-off of the absolute value of this amplitude with Q^2 whereas the NRCQM, as well as relativized versions, predict a much weaker fall-off or even an initial rise with Q^2. Experimental information about electroproduction amplitudes of the $P_{11}(1440)$ is rather limited, largely due to the complete lack of polarization data, and definite conclusions about

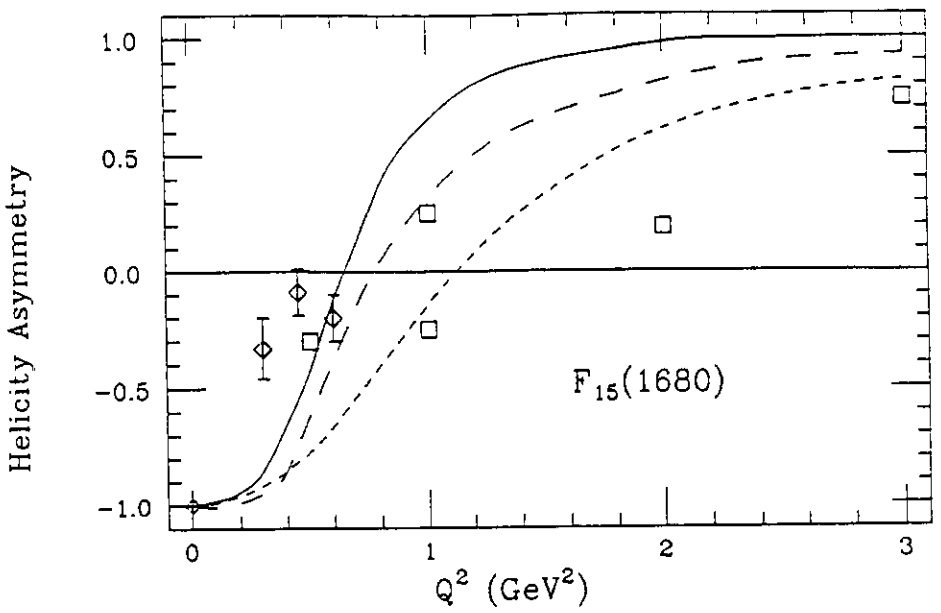

Figure 24. *Helicity asymmetry for the $\gamma_v pF_{15}(1688)$. NRCQM calculation by Ono[36] - long dashed line, Copley[37] - short dashed, Close[33] - solid, with QCD mixing.*

the nature of the $P_{11}(1440)$ will have to wait for more accurate data. The non-relativistic quark model predicts for the neutron/proton ratio: $A^n_{1/2}/A^p_{1/2} = -2/3$. In chiral bag model calculations[42] contributions from the pion cloud of the proton bring this ratio closer to -1 at $Q^2 = 0$. With increasing Q^2, however, the role of the pion cloud should be diminished, and the quark composition is expected to dominate the excitation of the $P_{11}(1440)$ at higher Q^2. Precise data on photo- and electro-excitation of the $P_{11}(1440)$ would help to reveal the true nature of this state. An interesting consequence of the $[56, 0^+]_2$ assignment of the $P_{11}(1440)$ is its predicted dominance over the $P_{33}(1232)$ at high Q^2. The NRCQM predicts[37]:

$$\frac{A_{1/2}(P_{11}(1440))}{A_{1/2}(P_{33}(1232))} \propto \vec{Q}^2 \quad . \tag{27}$$

The data are shown in Figure 25. The value -2/3 is preferred for the neutron/proton ratio, although a value closer to -1 is not ruled out. The Q^2 dependence is not well determined, however it is rather obvious that none of the explicit quark models comes even near to describing both the photon point and the Q^2 behaviour suggested by the data. Relativistic corrections give uncomfortably large effects, casting some doubts their convergence. The $P_{11}(1440)$ is predicted to couple rather strongly to longitudinal photons, a feature which is not supported by the data. $S_{1/2}$ is consistent with a small value, or even zero, although significant values at small Q^2 cannot be excluded. Clearly, more precise and more complete data are needed to study the apparently strong Q^2 dependence of $A_{1/2}$ at small Q^2, and to establish more accurate values for the longitudinal coupling.

Gluonic Excitations of the Nucleon

From inclusive lepton scattering experiments we know that in the deep inelastic

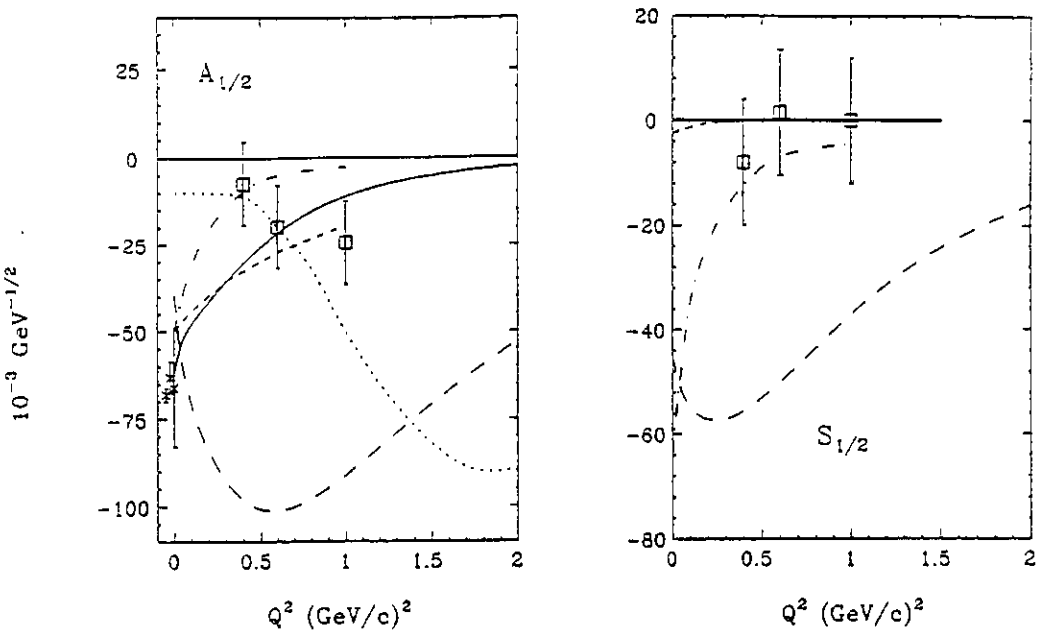

Figure 25. *Transverse (left) and longitudinal (right) photocoupling amplitudes of the $P_{11}(1440)$ for proton targets. The open symbols and the short dashed and dashed-dotted lines represent results of a fixed-t dispersion relation fit by Gerhardt*[44]. *Long dashes represent calculations for protons within the NRQM with QCD mixing*[33]. *The dotted line includes higher order relativistic corrections*[18]. *The solid lines are the result of a calculation assuming the $P_{11}(1440)$ is the gluonic partner of the nucleon*[43]. *Only calculations that approximately reproduce the photon point have been included.*

region about 50% of the proton momentum is carried by gluons. This raises the question of what impact gluons have on baryons spectroscopy. For example, can gluonic degrees of freedom be excited explicitly and generate new spectroscopic states? For some time there have been speculations about the existence of gluonic baryon states q^3G consisting of three constituent quarks and one constituent gluon[10],[11]. QCD lattice simulations indicate that such configurations may exist for mesons, whereas no such calculations have been performed for baryons. Estimates within the framework of bag models yield masses for the lowest P_{11}^G state around 1.5 GeV.

How can one search for these states? In hadronic production experiments gluonic baryons cannot be distinguished from ordinary q^3 states because they are, unlike gluonic mesons, characterized by quantum numbers which are also possible for the normal q^3 baryon states. However, as their internal structure is quite different from ordinary baryons, electroproduction experiments could be a powerful tool in these studies.

The $P_{11}(1440)$ has been suggested as a candidate for the gluonic partner of the nucleon[43]. The wave function for a nucleon with gluonic degrees of freedom may be written as:

$$|N>=\frac{1}{\sqrt{1+2\delta^2}}[|N_0> -\delta(|^4N_g> +|^2N_g>)] \ ,$$

where $|N_0>$ represents the wavefunction of the 3-quark system, which transforms as a [**56**] under $SU(6)$ for nucleons, $|^2N_g>$ and $|^4N_g>$ are the wave functions of the

q^3G system with the spin $\frac{1}{2}$ and $\frac{3}{2}$, respectively. The parameter δ is determined by the quark-gluon interaction. The corresponding state orthogonal to the nucleon in spin-flavor space is:

$$|N', J = \tfrac{1}{2} >= \sqrt{\tfrac{2}{1+2\delta^2}}[\delta|N_0 > + \tfrac{1}{2}(|^2N_g > + |^4N_g >)] \ .$$

It turns out that this description allows preservation of the successes of the quark model, most notably the neutron/proton ratio $A^n_{1/2}/A^p_{1/2} = -2/3$. If the $P_{11}(1440)$ were indeed the gluonic partner of the nucleon, a long-standing problem in baryon structure, the strong quenching of the transition formfactor $\gamma_v p P_{11}(1440)$ with Q^2 could be resolved. Obviously, the solution of the puzzle concerning the correct assignment of the $P_{11}(1440)$ could have enormous impact on our understanding of baryon structure and the dynamics of the strong interaction in the non-perturbative regime.

How can we experimentally discriminate between these alternatives? In a model of the nucleon containing constituent quarks and gluon, a graph that is expected to contribute to gluonic excitations is the QCD Compton process $\gamma q \to Gq$ (Figure 26)

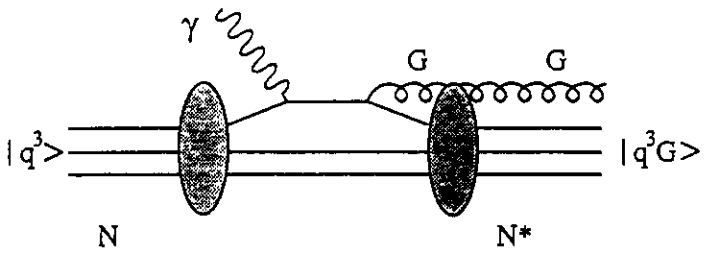

Figure 26. *QCD Compton process in gluonic excitation.*

The inverse process $gq \to \gamma q$, where g is an elementary gluon, has been studied in detail in hard scattering processes[45] and is well described in perturbative QCD. If the $P_{11}(1440)$ is a q^3G state, then, because the gluon has only transverse excitation modes the longitudinal coupling is absent, $\gamma_L p \not\to P_{11}$, and

$$S_{1/2}(Q^2) \equiv 0 \ . \tag{28}$$

This is consistent with the analysis of experimental data, although more accurate data especially at small Q^2 are needed for a more definite comparison.

A precise measurement of the Q^2 dependence of the $\gamma_v p P_{11}(1440)$ transverse photocoupling amplitude discriminates between the interpretation of the $P_{11}(1440)$ as a regular $[56, 0^+]_2$ q^3 state, or as a gluonic excitation where the 3-quark system transforms like a **[70]** under $SU(6)$. The discriminating power is a result of the fact that the respective photocoupling amplitudes are associated with different spin flavor factors for different spectroscopic assignments, so that in the first approximation (if effects from the spatial wavefunction and relativistic corrections are neglected):

$$\frac{A_{1/2}(P^G_{11})}{A_{1/2}(P_{11})} \sim \frac{1}{\vec{Q}^2} \ . \tag{29}$$

From (27), (28), and (29) one infers that a P^G_{11} state behaves like the $P_{33}(1232)$. Accurate measurement of the Q^2 dependence of the $P_{11}(1440)$ photocoupling amplitude can be used to discriminate between different spectroscopic assignments. The

calculation based on the q^3G interpretation is in better agreement with the data than calculations using the non-relativistic or relativized versions of the constituent quark model (Figure 25).

If the $P_{11}(1440)$ is the gluonic partner of the nucleon, then other gluonic states such as P_{13}^G, , P_{31}^G, P_{33}^G must exist as well, with masses around 1.6 - 1.7 GeV. The first two states have no place in the q^3 model at such low masses, whereas the latter one is also expected as a q^3 state. There is weak evidence for $P_{13}(1540)$ and $P_{31}(1550)$ states. Another question is, what would the mass of the lowest q^3 P_{11} be? The $P_{11}(1710)$ might be this state. Its mass is also more in accord with the NRCQM estimate. If this were the case, then the photocoupling amplitudes should exhibit a Q^2 dependence characteristic of a radially excited q^3 state.

Missing q^3 Baryon States

The QCD motivated extensions of conventional quark models predict many states with masses above 1.8 GeV which have not been observed in $\pi N \rightarrow \pi N$ reactions. Calculations[7] show that many of the "missing" states tend to decouple from the πN channel due to mixing, however, they may couple with significant strength to channels such as ρN, ωN, or $\pi\Delta$. It is experimentally well established that single pion production decreases with energy, while multi-pion production and vector meson production processes become more important (Figure 27). Electromagnetic production of these channels may therefore be the only way to study the "missing" states. In fact, several of those in the $[56, 2^+]_2$ super multiplet are predicted to couple strongly to photons. For example, the $F_{15}(1955)$, and the $F_{35}(1975)$ should be excited almost as strongly as some of the prominent states at lower masses. Search for these states is important and urgent. There are models, such as the quark cluster model[9] that can accommodate known baryon states, while predicting a fewer number of unobserved states. Future experiments[46],[47] to study electroproduction and photoproduction of vector mesons should provide a definite answer regarding the existence of at least some of these states. Figure 28 shows the predicted effect of one of the "missing" resonances on the differential cross section in $ep \rightarrow ep\omega$. At forward angles the process is dominated by diffractive production and the pion exchange diagram, while resonance contributions would dominate at backward angles. Similar behavior is expected for $ep \rightarrow ep\rho^0$, while $ep \rightarrow en\rho^+$ has no diffractive contributions and is more sensitive to resonant production.

Baryon Resonance Transitions at High Q^2

At high energies, perturbative QCD makes simple predictions about the asymptotic Q^2 behavior of the helicity amplitudes for resonance excitation. Based on the model of Brodsky and Lepage[48], who factorize the process into a hard scattering part and a 'soft' non-perturbative part described by quark distribution functions, it is expected[15] that

$$A_{1/2}(Q^2) = \frac{C_1}{Q^3}, \; A_{3/2}(Q^2) = \frac{C_2}{Q^5}, \quad Q^2 \rightarrow \infty \quad , \tag{21}$$

if logarithmic terms are neglected. Information about the quark distribution functions and the normalization constant C_1 may be obtained from QCD sum rules.

Of course, the first question to address is: At what momentum transfer does this description apply? Some interpretations[15] of the inclusive data have suggested

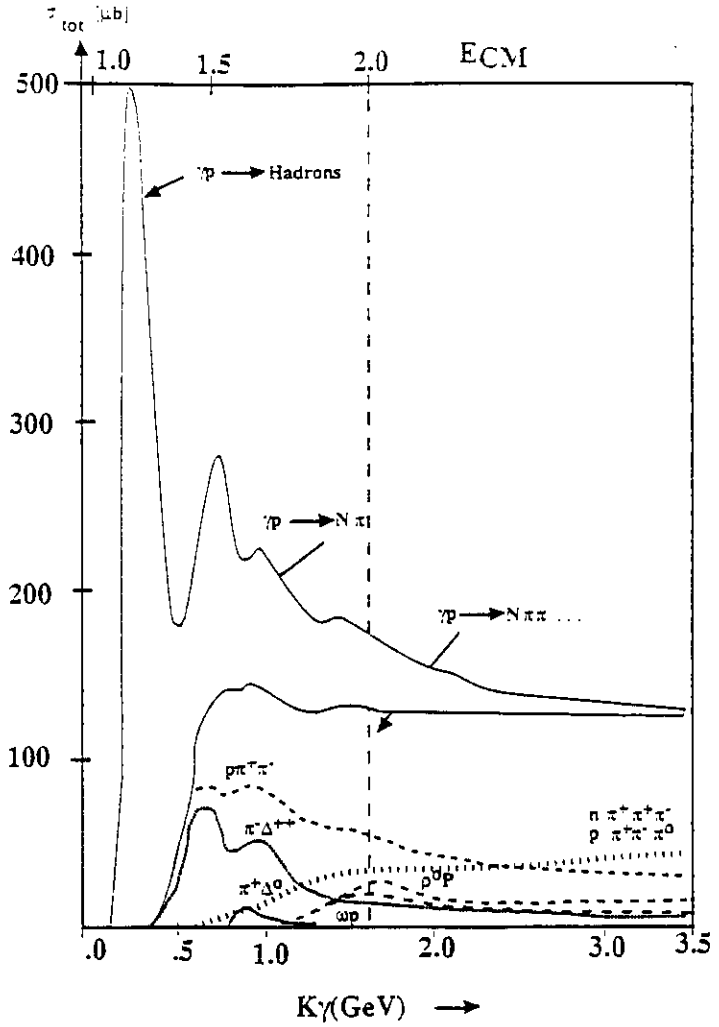

Figure 27. *Photoabsorption and total photoproduction cross section for various exclusive channels.*

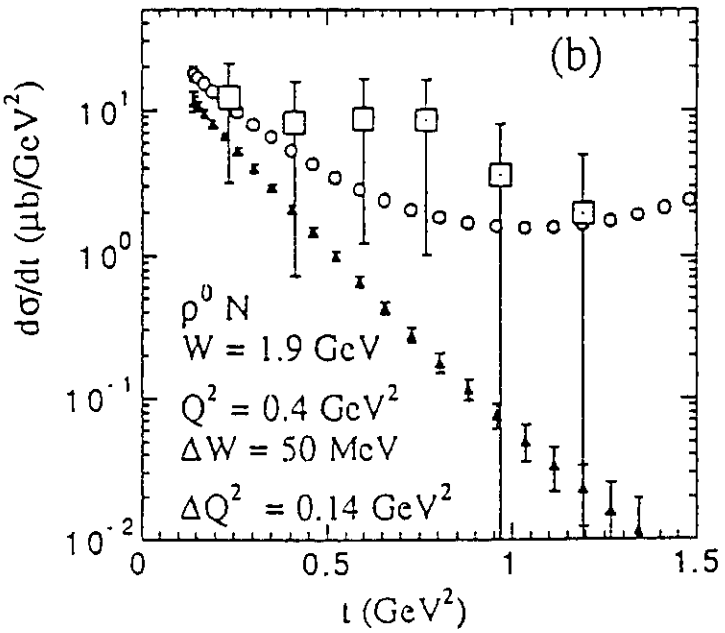

Figure 28: *Differential cross section for $\gamma_v p \rightarrow \rho^0 p$. Existing data (large errors), and projected data for a CEBAF experiment*[46] *are shown; full triangles without, open circles with the "missing" $F_{15}(1950)$ state.*

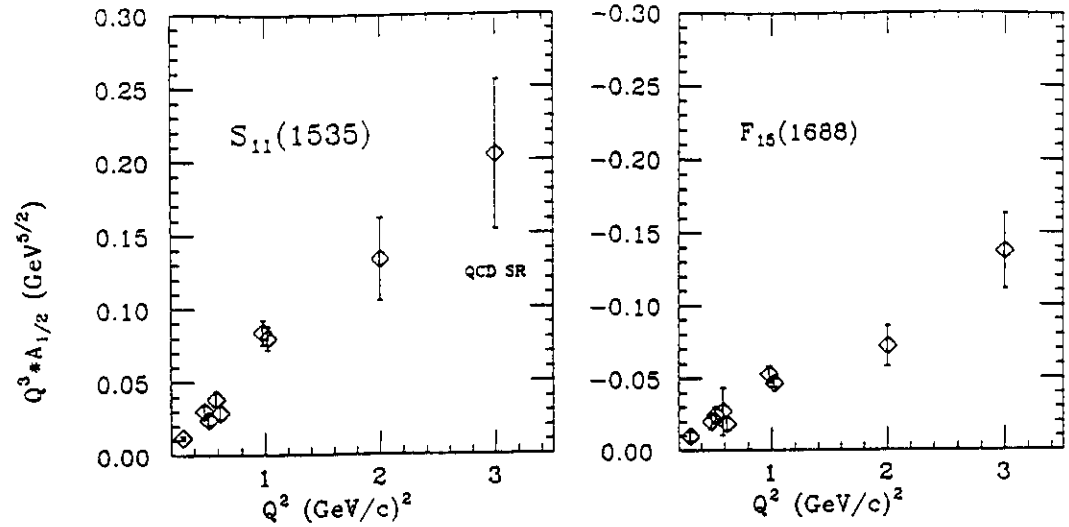

Figure 29. $Q^3 \cdot A_{1/2}$ *for various resonance transitions. The range of normalized QCD sum rule predictions of Carlson*[15] *for the asymptotic behavior of the* $\gamma_v p S_{11}$ *transition are indicated as lines labeled QCD SR.*

that the asymptotic behavior already is observed at $Q^2 \approx 4$ to 5 GeV^2. However, others[4,9] have argued that asymptotic behavior will occur only at much higher Q^2. Conclusive tests require exclusive data, where the resonances are uniquely identified, and their respective helicity amplitudes have been separated. Separated data exist for $Q^2 \leq 3GeV^2$ only, and only for a few states. In Figure 29 the $A_{1/2}$ data are shown, multiplied by Q^3. The onset of the asymptotic regime would be indicated by the Q^2 independence of this quantity. This is obviously not the case for this limited Q^2 regime.

Multiple quark transitions

It is well known[50] that q^3 baryon states belonging to the $[20, 1^+]$ super multiplet with its antisymmetric wave function cannot be excited from the ground state in a single quark transition. Search for direct electromagnetic excitation of these states allows direct tests of the SQT hypothesis. Calculations within the framework of a relativized quark model[18] indicate that multi quark transition (MQT) amplitudes may contribute at a level of 10 to 20% of those for SQT amplitudes of some of the prominent states. Search for these transitions requires high statistics measurements under conditions where interferences of the MQT amplitudes with other dominant amplitudes are important.

Nucleon Resonances and Spin Structure Functions

The results of the EMC measurements[51] on the polarized proton structure functions have prompted numerous speculations about whether or not in the deep-inelastic region the spin of the proton is carried by the quarks. Recent results from the CERN Spin Muon Collaboration (SMC)[52] and SLAC experiment E142[53] on the neutron polarized structure functions added additional speculations including one interpretation the neutron spin is not carried by quarks either. In another interpretation, the (fundamental) Björken sum rule[54] would be violated while leaving the (less fundamental) Ellis-Jaffe sum rule[55] for the neutron intact. The experiments on the neutron use data sets with Q^2 as low as 1 GeV^2. While such low Q^2 values have been

used in the analysis of unpolarized lepton scattering, there is a lack of convincing evidence that polarized structure functions exhibit true scaling behavior at such low Q^2. One should also keep in mind that the various spin sum rules are only defined at fixed Q^2 while the experiments integrate over large ranges in Q^2 . Moreover, the W range used in these analyses ($W \geq 2\ GeV$) may overlap part of the resonance region. The general perception is that for $W \geq 2\ GeV$ one probes the deep inelastic and hence scaling regime. However, excited nucleon states with masses as high as 3.0 GeV have been observed, and many states are predicted to exist in the mass region above 2.0 GeV, which raises the interesting question of how to correct for contributions resulting from these states. As the conclusion about the spin of the proton not being carried by quarks rests on relatively small differences between theoretical predictions and the data, it is important to study such contributions before far-reaching conclusions about the origin of the nucleon spin are drawn.

In some interpretations of the EMC results it is assumed that the missing quark spin may be accounted for by the so-called axial anomaly[56]. However, such contributions are rather controversial [57]. Another possibility is that most of the proton spin resides in orbital angular momentum contributions. Such contributions are necessarily associated with extended objects and therefore cannot be probed in deep inelastic scattering, however, they may be accessible at lower energies and momentum transfers. The low Q^2, and low energy loss ν region may therefore contain significant information about the spin structure of the nucleon. This is the kinematical regime where contributions from excited N^* and Δ^* resonances are important.

Polarized Structure Functions of the Proton

The spin-structure of the proton is usually discussed in relation to the deep-inelastic polarized structure functions $g_1(x)$ and the first moment $\Gamma = \int g_1(x)$. In the kinematical regime of resonances, and at low Q^2, use of total helicity $\frac{1}{2}$ and $\frac{3}{2}$ photon-nucleon absorption cross sections is more convenient.

The sum rule by Gerasimov[58], and independently by Drell and Hearn[59] relates the difference in the total photoabsorption cross section on nucleons for $\lambda_{\gamma N} = \frac{1}{2}$ and $\lambda_{\gamma N} = \frac{3}{2}$ to the anomalous magnetic moment of the target nucleon.

$$I_p(0) = \frac{M_p^2}{8\pi^2\alpha} \int_{\nu_{thr.}}^{\infty} \frac{d\nu}{\nu}(\sigma_{1/2}^p(\nu) - \sigma_{3/2}^p(\nu)) = -\frac{1}{4}\kappa^2 \quad , \tag{31}$$

where κ is the anomalous magnetic moment of the target nucleon. Assuming scaling behavior the EMC results can be written as:

$$I_p(Q^2) = \frac{2M_p^2}{Q^2}\Gamma_p^{EMC} \simeq \frac{0.222 \pm 0.018 \pm 0.026}{Q^2} \tag{32}$$

where QCD corrections have been neglected. $I_p(0)$ is large and negative, whereas the EMC data yield a positive $I_p(Q^2)$. In order to reconcile the GDH sum rule with the EMC results, dramatic changes in the helicity structure must occur when going from $Q^2 = 0$ to finite values of Q^2. In an analysis of photoproduction data[60],[61] for energies up to $E_\gamma = 1.7\ GeV$ single pion production contributions were found to nearly saturate the sum rule. An analysis of electroproduction data[62] including known resonant channels as well as non-resonant single pion Born terms showed that contributions of the $P_{33}(1232)$ to $I_p(Q^2)$ are dominant at small Q^2. This analysis also

Measurement of the single pion cross section allows the determination of four response functions σ_T, σ_L, σ_{TT}, σ_{TL} in (13), which are functions of the helicity amplitudes H_i. Measurement of polarization observables yields information on many response functions (table 3). While measurement of the unpolarized response functions allows determination of prominent resonance transitions, the weaker transitions are difficult to determine in such a way.

Table 3: Response functions in pion electroproduction.

Experiment	# Response Functions
$eN \rightarrow eN'\pi$	4
$\vec{e}N \rightarrow eN'\pi$	1
$e\vec{N} \rightarrow eN'\pi$	8
$\vec{e}\vec{N} \rightarrow eN'\pi$	5
$eN \rightarrow e\vec{N}'\pi$	8
$\vec{e}N \rightarrow e\vec{N}'\pi$	5

Since polarization observables contain interference terms between amplitudes they are sensitive to small amplitudes and to relative phases between amplitudes. Even measurements of limited statistical accuracy will be extremely important in determining absolute values and signs of small amplitudes which are otherwise not accessible. Not all the response functions contain independent information. In particular, only four of the response functions measured with a polarized target are different from the ones measured with recoil polarimeters. In many applications the two methods can be quite competitive, which allows one to select the more convenient technique.

Figure 31 shows the sensitivity of the unpolarized cross section for $p(e,e'p)\pi^0$ and the target asymmetry T_{long} to the excitation strength of the $P_{11}(1440)$. As the transition amplitudes of the $P_{11}(1440)$ may be quite small, the sensitivity of polarization experiments is essential in measuring these amplitudes. Similar sensitivities to the $P_{11}(1440)$ amplitudes have been found in measurements of the proton recoil polarization[64] in $p(e,e'\vec{p})\pi^0$.

The main objective is to disentangle the various resonant partial waves. This requires measurement of complete angular distributions with respect to the direction of the virtual photon. Also, measurements in different isospin channels are needed to separate resonant and non-resonant amplitudes with different isospin assignments. Complete isospin information can be obtained from a study of the reactions

$$\gamma_v + p \rightarrow p + \pi^0$$

$$\gamma_v + p \rightarrow n + \pi^+$$

$$\gamma_v + n \rightarrow p + \pi^- \quad .$$

In addition, measurement of

$$\gamma_v + p \rightarrow p + \eta$$

selects isospin 1/2, and is a unique means of tagging the $S_{11}(1535)$ and the $P_{11}(1710)$ resonances which both have a significant coupling to the $N\eta$ channel.

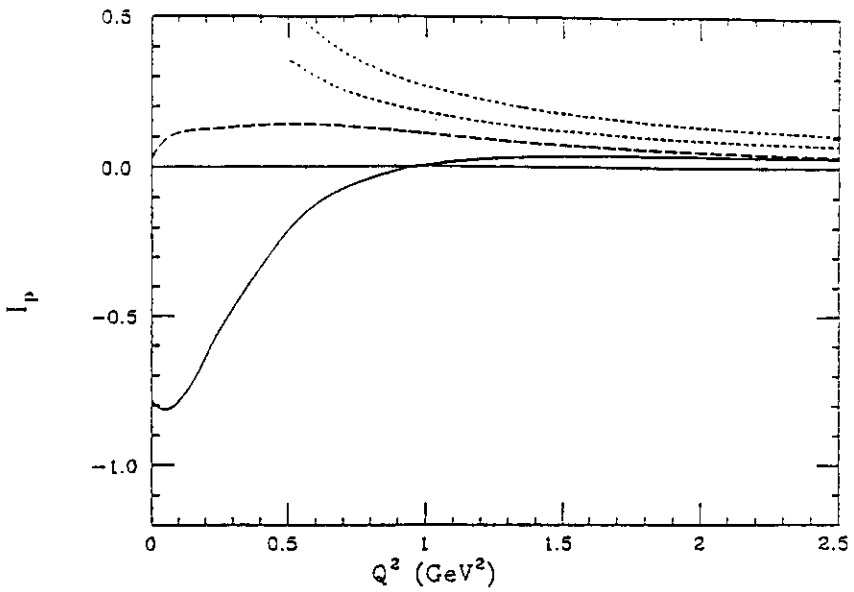

Figure 30. *The integral $I_p(Q^2)$. The solid curve represents the results of the empirical analysis by Burkert and Li*[62]*. The long dashed line is the result of the same analysis excluding the $P_{33}(1232)$ contribution. The short dashed lines represent the extrapolated EMC results.*

showed that contributions from other resonances become significant with increasing Q^2, in fact causing $I_p(Q^2)$ to change its sign at Q^2 between 0.5 to 1.0 GeV^2. Resonance contributions other than the $P_{33}(1232)$ contribute as much as 50% or more of the extrapolated EMC results at $Q^2 = 1\ GeV^2$ (Fig. 30), which highlights the importance of the nucleon resonance region for a full understanding of the nucleon spin structure.

AN EXPERIMENTAL STRATEGY

In a discussion of the experimental aspects it is useful to distinguish baryon resonance studies according to the complexity of the final state.

Single Pion and Eta Production

Most of the existing data consist of differential cross sections of single π or η production using unpolarized beams and targets. This channel is particular sensitive to the lower mass resonances ($W \leq 1.7\ GeV$) which decay dominantly into the πN channel, or in the case of the $S_{11}(1535)$ into ηN. Much of the theoretical formalism required for data analysis has been worked out for these channels. In single pion electroproduction from nucleons, 11 independent measurements are needed at a given kinematical point (Q^2, W, θ_π) to determine the amplitudes of the process $\gamma_v N \rightarrow N'\pi$ in a model independent fashion. The complete determination of the transition amplitudes in pion and eta production over a large kinematical range is the ultimate goal of nucleon resonance physics with electromagnetic probes. This program requires high statistics measurements of unpolarized cross sections, and detailed measurements of polarization observables using polarized beams, polarized nucleon targets, and the measurement of nucleon recoil polarization.

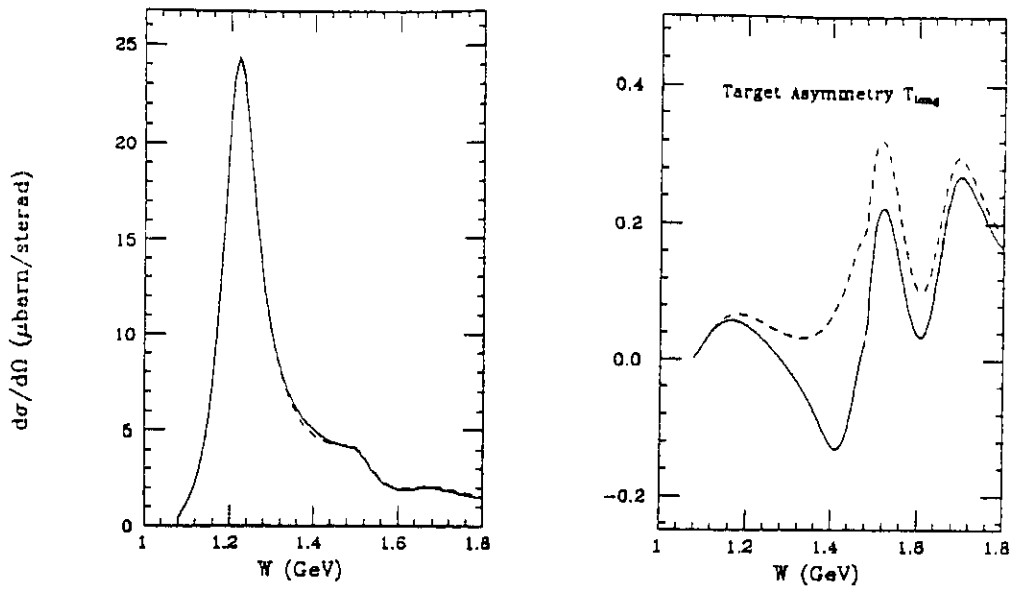

Figure 31. *Predicted cross section (left) for* $\gamma_v p \rightarrow p\pi^0$ *at* $Q^2 = 0.25 GeV^2$, $\epsilon = 0.8$, $\theta_\pi^* = 90^o$, $\phi_\pi = 30^o$. *The AO code*[66] *amplitudes were used. Predicted target asymmetry for target polarization along the incident electron beam* T_{long} *for the same kinematics (right). The sensitivity to the amplitudes of the* $P_{11}(1440)$ *resonance is shown: solid line - with* P_{11}, *dashed line - without* P_{11}.

The various experimental requirements call for an experimental setup which allows measurement of complete angular distributions in different isospin channels simultaneously.

Multiple Pion Production.

For higher masses, multiple pion production due to decay channels such as $\pi\Delta$, ρN, and ωN becomes the dominant process. For example, the $S_{31}(1650)$ and $D_{33}(1700)$ decay about 70% and 85% of the time, respectively, into the $N\pi\pi$ channel, with dominant contributions coming from the $\pi\Delta$ decay. Obviously, a study of baryon resonance production in this mass region requires measurement of these channels. The information that can be extracted from the two-pion process is potentially very rich since polarization observables can be measured in the final state. For example, the measurement of the $\Delta \rightarrow N\pi$ decay allows a determination of the Δ helicity in the process $\gamma p \rightarrow \Delta\pi$. This should prove very powerful in determining the resonant contributions to the process. Moreover, clarification of the existence of states such as $P_{13}^G(1540)$ and $P_{31}^G(1550)$ also appears more promising in the multi-pion channel than in single pion production.

Experimental Equipment

A comprehensive and efficient experimental program to study electromagnetic transitions of baryon resonances in a large kinematical region, requires experimental equipment with large solid angle coverage, the capability to measure neutral particles, and compatibility with polarized proton and neutron targets. At CEBAF, a large acceptance spectrometer (CLAS) based on a toroidal magnetic field is un-

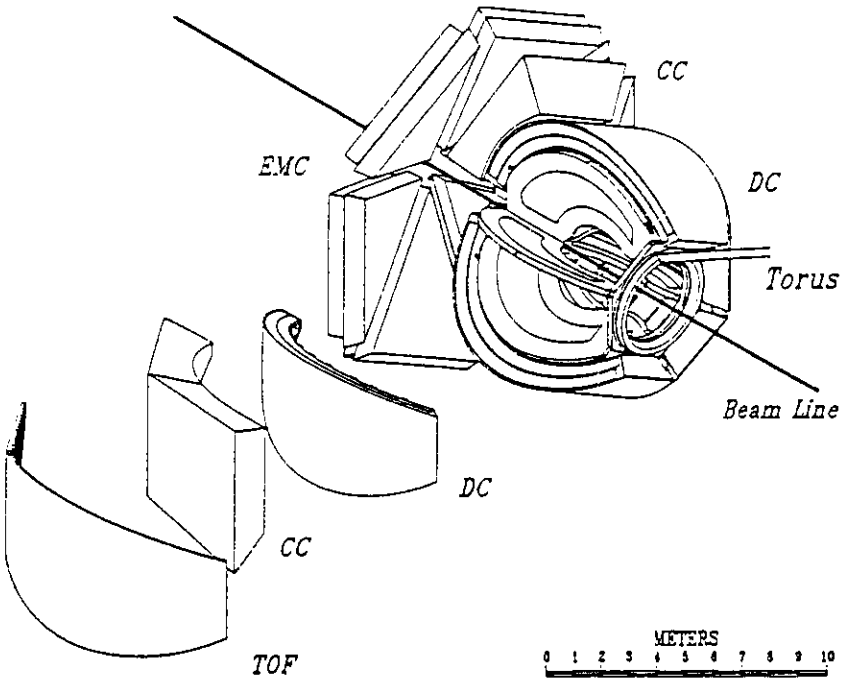

Figure 32. *The CEBAF Large Acceptance Spectrometer (CLAS)*[6]. *Six symmetrically arranged superconducting coils generate an approximate toroidal magnetic field. Drift chambers, time-of-flight counters, gas Cerenkov counters, and an electromagnetic calorimeter provide particle identification, charged particle tracking, and energy measurements for electromagnetic particles. The field free region around the target allows use of polarized solid state targets.*

der construction[6]. A significant portion of the scientific program for this detector is aimed at studies of baryon resonance excitations using electron and photon beams[41]. Figure 32 shows an artists view of the CLAS spectrometer. As an example, Figure 33 shows a comparison of existing data in the $P_{33}(1232)$ region with projected data expected from measurements with CLAS.

Many details of baryon resonance excitations, in particular at lower masses, may be addressed with magnetic spectrometers, which have small solid angles, but are able to operate at very high luminosities. Single pion production near pion threshold and in the $P_{33}(1232)$ region, or eta production in the $S_{11}(1535)$ region could be measured with high precision. Small solid angle, high rate magnetic spectrometers may also allow accurate measurements of proton recoil polarizations in reactions such as:

$$e + p \rightarrow e + \vec{p} + \pi^0$$

$$e + n \rightarrow e + \vec{p} + \pi^-$$

$$e + p \rightarrow e + \vec{p} + \eta.$$

Polarization experiments with such spectrometers are in preparation at CEBAF, at MIT-Bates, and at MAMI-B. These are designed to make precise measurements of single π^0 production off protons in the $\Delta(1232)$ region, with the goal of extracting more accurate information about the small E_{1+} and S_{1+} multipoles.

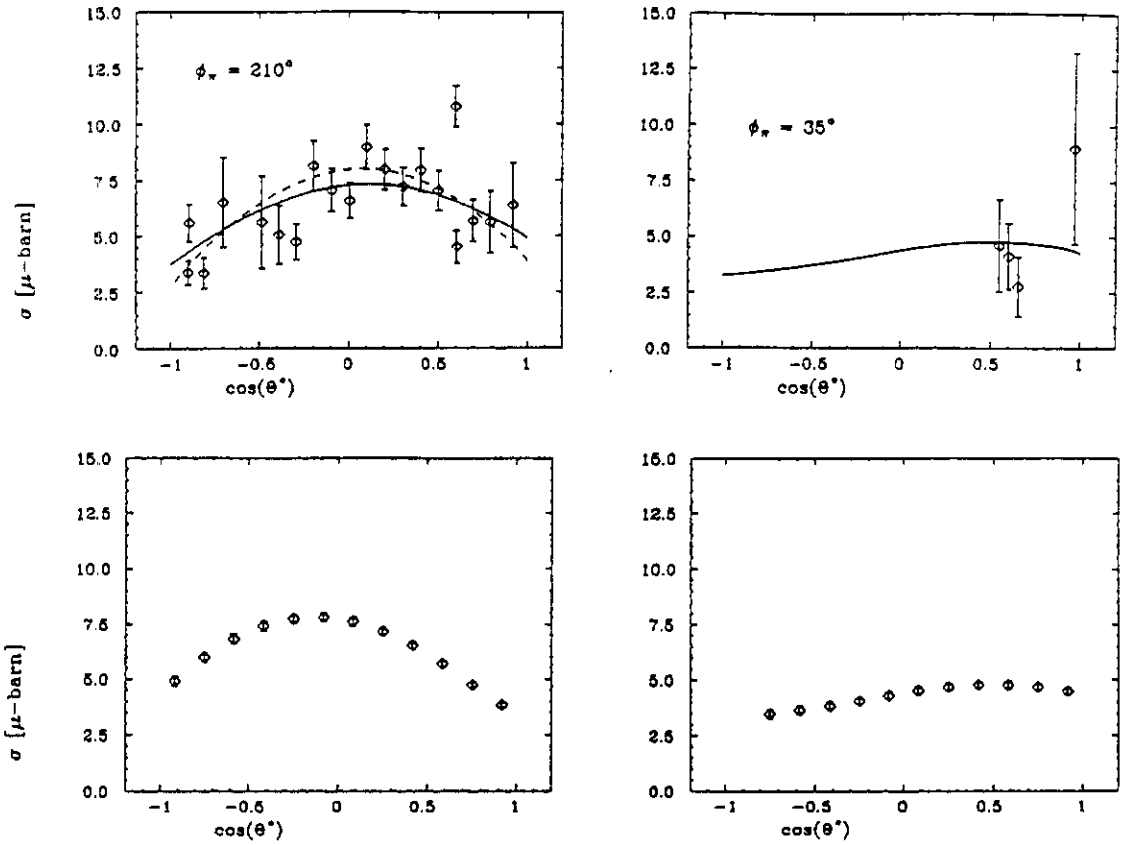

Figure 33. *Differential cross section for π^0 and π^+ production from protons (top), and projected data from CLAS (bottom). A 1000 hour run at a luminosity of 10^{34} $cm^{-2}sec^{-1}$ has been assumed.*

OUTLOOK

In the past, studies of the structure of baryons using electromagnetic excitation of nucleon resonances have suffered from several shortcomings. Firstly, theoretical guidance based on models which have some basis in the theory of strong interaction was established only after the bulk of the experiments had been completed. Secondly, all of the high statistic experiments are single pion production measurements. In view of QCD based quark models, this allows the study of lower mass states with a large elasticity. However, single pion production measurements are not suited for the study of most of the higher mass states. These are predicted to largely decouple from the πN channel, which makes this channel insensitive to resonance excitation in the higher mass region. Thirdly, the notorious rate problem in electromagnetic production experiments prevented high statistics measurements to be performed, even in the case of single pion production.

The construction of continuous electron accelerators in the multi-GeV range, and the utilization of large acceptance detectors has opened up the possibility of studying the structure of the nucleon with unprecedented accuracy. The analysis of this data,

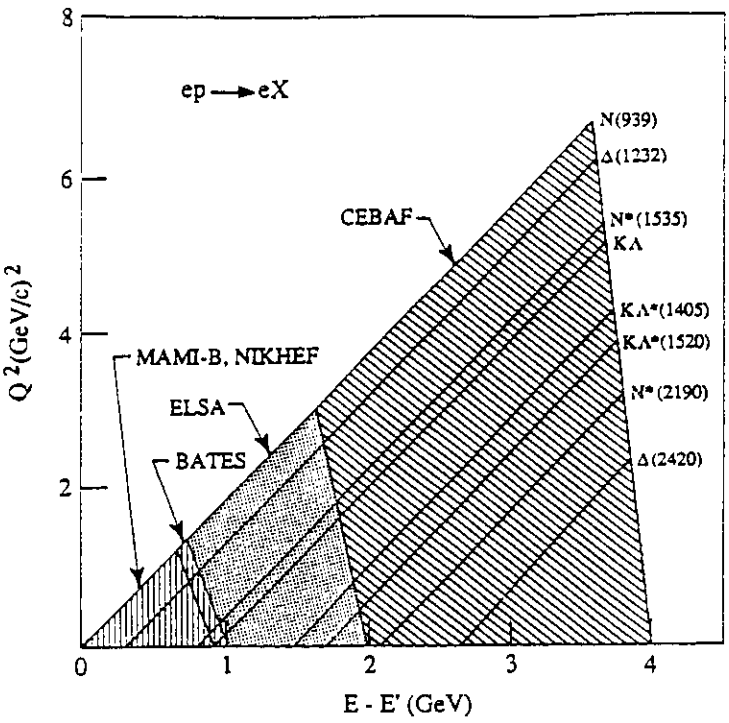

Figure 34. *Kinematical region accessible at various CW electron machines.*

and the comparison with theoretical descriptions of the nucleon in terms of quarks and gluons will give us detailed insight into the dynamics of hadronic systems and the underlying strong interaction force.

Several new CW electron accelerators in the GeV and multi-GeV range are now under construction. Figure 34 shows the resonance mass range accessible with these machines covering the entire nucleon resonance mass region and a large Q^2 range. Clearly, with these machines, and with the use of modern experimental equipment, the scientific community will have powerful new instruments which will allow for progress on many of the outstanding problems in baryon structure and strong interaction physics.

References.

[1] N. Isgur, G. Karl, *Phys. Lett. 72B, 109 (1977); Phys. Rev. D23, 817 (1981).*

[2] S. Capstick, N.Isgur, *Phys. Rev. D34, 2809 (1986); S. Capstick, Phys. Rev. D36, 2800 (1987)*

[3] S. Capstick, *Phys. Rev. D46,2864(1992)*

[4] F. Iachello, *Phys. Rev. Lett. 62, 2440 (1989)*
R. Bijker and A. Leviatan, *Proceedings of 6th Workshop on Nuclear Physics at Intermediate Energies, Trieste, May 3 - 7, 1993.*

[5] G. Eckart and B. Schwesinger , *Nucl. Phys. A458, 620 (1986)*

[6] V. Burkert and B. Mecking, *Large Acceptance Detectors for Electromagnetic Nuclear Physics*, in: *Modern Topics in Electron Scattering*, eds. B. Frois, I. Sick, *World Scientific, Singapore, 1991.*

[7] Particle Data Group, Review of Particle Properties, *Phys. Rev.D45 (1992).*

[8] R. Koniuk, N. Isgur, *Phys. Rev. D21, 1868 (1980)*
[9] K.F. Liu, C.W. Wong, *Phys. Rev. D28, 170 (1983)*
[10] E. Golowich, E. Haqq, G. Karl, *Phys. Rev. D28, 160 (1983)*
[11] T. Barnes, F.E. Close, *Phys. Letts. 123B, 89 (1983)*
[12] R. Longacre, *Nucl. Phys. B211, 1 (1977)*
[13] P. Stoler, *Phys. Rev. Lett. 66, 1003 (1991)*
[14] M. Köbberling, et al., *Nucl. Phys. B82, 201 (1974)*
S. Stein et al., *SLAC-PUB-1518 (1975)*
[15] C.E. Carlson, *Phys. Rev. D34, 2704 (1986)*
C.E. Carlson, J.L. Poor,*Phys. Rev. D38, 2758 (1988)*
C.E. Carlson, *Proc. 12th Internat. Conf. on Few Body Problems*
[16] K. Bätzner et al., *Phys. Lett. 39B, 575 (1972)*
[17] J. Drees et al., *Z. Phys. C7, 183 (1981)*
[18] M. Warns et al., *Z. Phys.C45, 627 (1990)*
[19] F. Foster, G. Hughes, *Z. Phys. C14, 123 (1982)*
[20] H.F. Jones and M.D. Scandron, *Ann. Phys. 81, 1 (1972)*
[21] G. Baum et al.; *Phys. Rev. Lett. 45, 2000 (1980)*
[22] V. Eckardt, et al., *Nucl. Phys. B55, 45(1973)*
K. Wacker et al., *Nucl. Phys. B144, 269 (1978)*
[23] K. Bätzner et al., *Nucl. Phys. B75, 1 (1974)*
[24] R. Lourie, V. Burkert, (co-spokesmen), *Bates Proposal PR 89-03;*
C. Papanicolas et al., *Bates Proposal PR 87-09*
[25] *CEBAF Proposals PR 89-37 and PR 89-42 of the N^* collaboration*
[26] R.L. Walker, *Phys. Rev. 182, 1729 (1969)*
[27] R.G. Moorhouse, in: *Electromagnetic Interaction of Hadrons Vol. 1, eds. A. Donnachie and G. Shaw, Plenum Press, 1978*
[28] D.H. Lyth, in: *Electromagnetic Interaction of Hadrons Vol. 1, eds. A. Donnachie and G. Shaw, Plenum Press, 1978*
[29] R. Haidan, *PhD Thesis, University of Hamburg; DESY Internal report No. F21-79/03 (unpublished)*
[30] K.H. Althoff et al., *Z. Phys. C1, 327 (1979)*
[31] H. Breuker et al., *Phys. Letts. 74B, 409 (1978)*
[32] W. Brasse et al., *Z. Phys. C22, 33 (1984)*
[33] F. Close and Z.P. Li, *Phys.Rev.D42, 2194(1990)*
[34] W. Konen and H.J. Weber, *Phys. Rev. D41, 2201 (1990)*
[35] C.P. Forsyth, J.B. Babcock, *Preprint CMU-HEP 83-4 (1983)*
[36] S. Ono, *Nucl. Phys. B107, 522 (1976)*
[37] L.A. Copley, G. Karl, E. Obryk, *Phys. Letts. 29B, 117 (1969)*
[38] F.E. Close, F.J. Gilman, *Phys. Letts. 38B, 541 (1972)*
F.E. Close, F.J. Gilman, I. Karliner, *Phys. Rev. D6, 2533 (1972)*
[39] H. Breuker et al., *Z. Phys. C17, 121 (1983)*
H. Breuker et al., *Z. Phys. C13, 113 (1982)*
[40] F. Foster and G. Hughes, *Rep. Prog. Phys., Vol. 46, 1445 (1983)*
[41] A.J.G. Hey, J. Weyers, *Phys. Letts. 48B, 69 (1974)*
W.N. Cottingham, I.H. Dunbar, *Z. Phys. C2, 41 (1979)*
[42] K. Bermuth, D. Drechsel, D. Tiator and J.B. Seaborn, *Phys.Rev.D37, 89 (1988)*
[43] Z.P. Li, V. Burkert, Z. Li, *Phys. Rev. D46, 70 (1992)*
[44] C. Gerhardt, *Z. Phys. C4, 311(1980)*
[45] V. Burkert, *Proceedings, 18th Rencontre de Moriond, January 23-29, 1983, La Plagne, pg. 189, Editions Frontières, ed. J. Tran Thanh Van*

[46] H. Funsten et al., *CEBAF Proposal 91-024 (1991)*
M. Ripani et al.. CEBAF Proposal 93-06, also: *Proceedings, Workshop on "Exclusive Reactions at High Momentum Transfer ", Elba, Italy, July 1993*
[47] D. Menze, Talk presented at the *Int. Workshop on Baryon Structure and Spectroscopy, Paris, September 22-25, 1991*
[48] S.J. Brodsky, G.P. Lepage, *Phys. Rev. D24, 2848 (1981)*
[49] N. Isgur and C.H. Llewellyn-Smith. *Nucl. Phys. B317 ,526 (1989)*
[50] R.P. Feynman, *Photon Hadron Interactions, Frontiers in Physics, W.A. Benjamin, Inc. (1972), pg.49*
[51] J. Ashman et al., *Phys. Lett. B206,(1988)364; Nucl. Phys.B328 (1989)1*
[52] B. Adeva et al.,*Phys. Lett. B302, 533 (1993)*
[53] P.L. Anthony et al. (E142 Collaboration); Presented at *PANIC '93, Perugia, Italy, June 1993*
[54] J.D. Björken, *Phys.Rev. 148, 1467(1966)*
[55] J. Ellis and R.L. Jaffe, *Phys. Rev. D9, 1444 (1974)*
[56] G. Altarelli, G.G. Ross, *Phys. Lett. B214, 381(1988)*; R. Carlitz, J.C. Collins, A.M. Mueller,*Phys. Lett.B214, 2229 (1988)*
[57] R. Manohar, in: *Polarized Collider Workshop, University Park, Pa. , 1990., AIP Conference Proc. No.223*
[58] S. Gerasimov,*Yad.Fiz.2, 598(1965) [Sov. J. Nucl. Phys. 2 (1966)930]*
[59] S.D. Drell and A.C. Hearn, *Phys. Rev. Lett. 16 (1966) 908*
[60] I. Karliner, *Phys.Rev. D7, 2717 (1973)*
[61] R. Workman and R. Arndt, *Phys. Rev. D45, 1789(1992)*
[62] V. Burkert and Zh. Li, *Phys. Rev.D47, 46(1993)*
[63] D. Drechsel, *6th Int. Workshop on Perspectives in Intermediate Nuclear Physics, Trieste, May 4 - 7, 1993*
[64] R. Lourie, *Z. Phys. C50, 345 (1991)*
[65] W. Albrecht et al., *Nucl. Phys. B27, 615 (1971)*
S. Galster et at., *Phys. Rev. D5, 519 (1972)*
R. Siddle et al., *Nucl. Phys. B35, 93 (1971)*
R. D. Hellings et al., *Nucl. Phys. B32, 179 (1971)*
J.C. Alder et al., *Nucl. Phys. B46, 573 (1972)*
K. Bätzner et al.,*Nucl. Phys. B75, 1 (1974)*
[66] V. Burkert and Zh. Li, *AO code, unpublished*